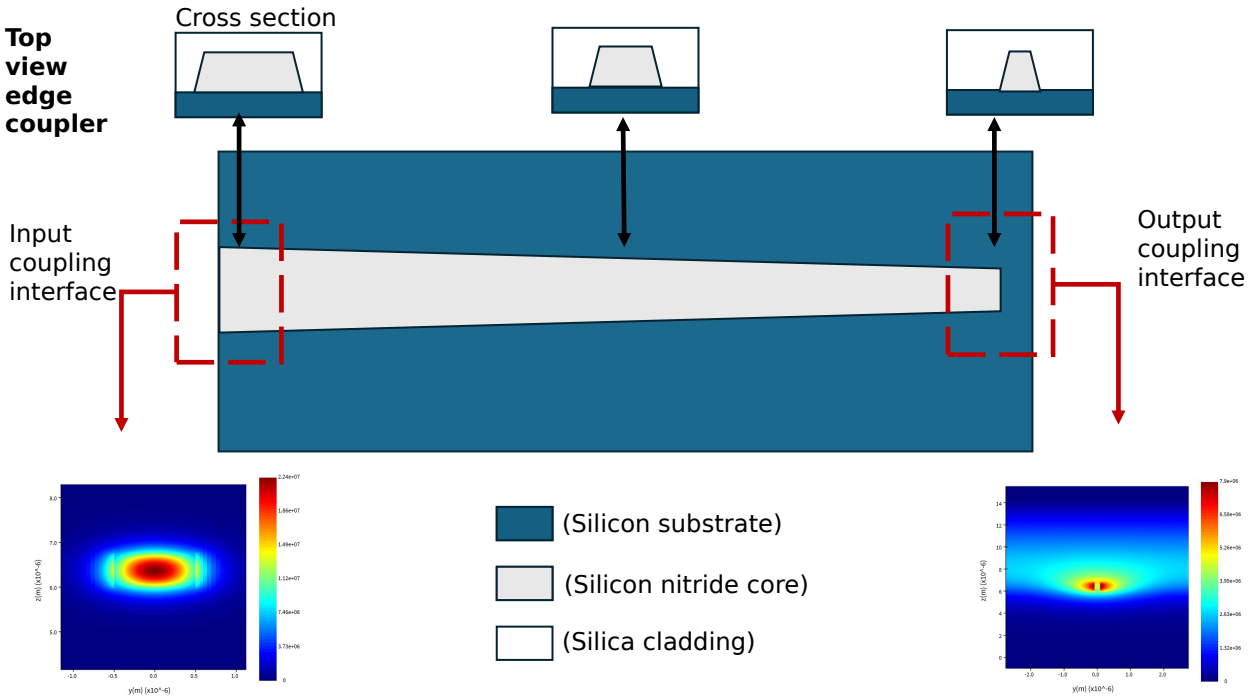

Optimization of coupling interfaces between nanophotonics waveguides and optical fibers

Master's thesis in Wireless , Photonics and Space Engineering

Ali Haidar Hussein

Department of Microtechnology and Nanoscience
CHALMERS UNIVERSITY OF TECHNOLOGY
Gothenburg, Sweden , 2024
www.chalmers.se

Master's thesis 2024

Optimization of coupling interfaces between nanophotonics waveguides and optical fibers

Design and Simulation of Edge Couplers for Enhanced Fiber-to-Chip Integration

Ali Haidar Hussein

CHALMERS
UNIVERSITY OF TECHNOLOGY

Department of Microtechnology and Nanoscience
Photonics Division
Integrated Ultrafast Photonics Group
Chalmers University of Technology
Gothenburg, Sweden 2024

Optimization of coupling interfaces between nanophotonics waveguides and optical fibers
Design and Simulation of Edge Couplers for Enhanced Fiber-to-Chip Integration in Photonic Systems
ALI HAIDAR HUSSEIN

Supervisor: Yan Gao and Vijay Shekhawat , Integrated Ultrafast Photonics Group
Examiner: Victor Torres Company, MC2 , Integrated Ultrafast Photonics Group

Master's Thesis 2024
MC2 Department
Photonics Division
Integrated Ultrafast Photonics Group
Chalmers University of Technology
SE-412 96 Gothenburg
Telephone +46 31 772 1000

Cover: Diagram of an edge coupler showing light coupling from an optical fiber into a waveguide via an edge interface with a tapered waveguide

Typeset in LaTeX
Printed by Chalmers Reproservice
Gothenburg, Sweden 2024

Optimization of coupling interfaces between nanophotonics waveguides and optical fibers
Design and Simulation of Edge Couplers for Enhanced Fiber-to-Chip Integration in Photonic Systems
ALI HAIDAR HUSSEIN
MC2 Department
Chalmers University of Technology

Abstract

The integration of photonic components into compact and efficient circuits necessitates effective coupling mechanisms between optical fibers and on-chip waveguides. This thesis focuses on optimizing the coupling efficiency between silicon nitride (Si_3N_4) waveguides and optical fibers using linear adiabatic edge tapers. Addressing the significant challenge of minimizing coupling losses, the study explores the interplay between taper geometry, cladding thickness, taper and physical gaps for both standard single-mode fibers (SMFs) and lensed fibers.
Utilizing both advanced simulation tools—Finite-Difference Eigenmode (FDE), Eigenmode Expansion (EME), and Finite-Difference Time-Domain (FDTD) methods—and experimental validation, the research systematically investigates the parameters influencing coupling efficiency. FDE simulations provide initial insights into mode mismatch losses due to mode field diameter (MFD) disparities. EME simulations are employed to optimize taper lengths, ensuring adiabatic mode transformation with minimal loss. FDTD simulations offer a comprehensive 3D analysis, capturing detailed electromagnetic interactions at the coupling interface. Experimental prototypes were fabricated and tested to validate the simulation results and assess practical fabrication considerations.
The results demonstrate that optimal coupling for SMFs is achieved with a taper length of approximately 1mm, a facet width between 100nm and 150nm (with 125nm yielding the lowest loss), and a cladding thickness of 6µm, resulting in coupling losses around 0.75dB. For lensed fibers, both simulations and experiments indicate that a taper length of 50µm, a facet width between 230nm and 290nm (with 290nm yielding the losses in the simulations around 0.37 dB per facet and an experimental loss of around 1.1dB per facet which is possible to reduce even further), and a cladding thickness of 3µm yield optimal coupling efficiency. The slight discrepancies between simulated and experimental results are attributed to fabrication imperfections, including sidewall roughness and taper dimension deviations.
The study underscores the critical impact of physical gaps and beam divergence on coupling efficiency, emphasizing the necessity of precise alignment and minimal separation in practical applications. Experimental results confirm that minimizing the taper and physical gaps is essential for lensed fiber coupling, with coupling losses yielding a constant value for gaps that are larger than 0.5µm.
The thesis identifies limitations related to fabrication imperfections and suggests avenues for future research, including broadband performance analysis and the incorporation of fabrication-induced variations into simulations. The findings offer valuable design considerations for enhancing fiber-to-chip coupling in Si_3N_4 pho-

tonic integrated circuits, contributing to the advancement of efficient and scalable optical communication technologies.

Keywords: (Silicon Nitride Si_3N_4) waveguides, Photonic Integrated Circuits, Linear Adiabatic Edge Tapers, Fiber-to-Chip Coupling, Single Mode Fibers, Lensed Fibers, Finite-difference time-domain ,Eigenmode Expansion, Mode Field Diameter

Acknowledgements

First and foremost, I would like to express my deepest gratitude to Professor Victor Torres for inviting me to join the Integrated Ultrafast Photonics Research Group and giving me the opportunity to carry out this research project. His guidance and support have been invaluable.
I am especially grateful to my supervisors, Yan Gao and Vijay Shekhawat, for their exceptional guidance and unwavering support throughout this research. I deeply appreciate their time, energy, and commitment, as well as the long hours we spent together for the sake of this project.
I would also like to extend my heartfelt thanks to the wonderful friends I made in Gothenburg, who made me feel at home throughout these two years. Thank you for all the memorable experiences we shared together.
Last but not least, I dedicate this thesis to my family—my father and mother—without whom none of this would have been possible. Their endless support through thick and thin has been my foundation. I am especially grateful to my beloved dad, who has always pushed me to strive for nothing less than excellence in life and in the quest for knowledge.

Ali Haidar Hussein, Gothenburg, 2024

List of Acronyms

Below is the list of acronyms that have been used throughout this thesis, listed in alphabetical order:

CAD	Computer-Aided Design
CMOS	Complementary Metal-Oxide-Semiconductor
EME	Eigenmode Expansion
FDE	Finite Difference Eigenmode
FDTD	Finite Difference Time Domain
LiDAR	Light Detection and Ranging
LPCVD	Low-Pressure Chemical Vapor Deposition
MFD	Mode Field Diameter
PIC	Photonic Integrated Circuit
PML	Perfectly Matched Layer
SEM	Scanning Electron Microscope
Si_3N_4	Silicon Nitride
SiO_2	Silicon Dioxide
SMF	Single-Mode Fiber
TE	Transverse Electric
TM	Transverse Magnetic

Contents

List of Figures

List of Tables

1

Introduction

1.1 Background on Photonic Integrated Circuits (PICs)

1.1.1 Definition and Significance

Photonic Integrated Circuits (PICs) represent a transformative advancement in the field of photonics, where multiple optical components, such as lasers, modulators, detectors, and waveguides, are integrated onto a single chip [1]. Similar to electronic integrated circuits (ICs), which have revolutionized the field of electronics by combining various electronic components into a compact, highly functional package, PICs aim to achieve a similar concept of integrating passive and active devices together but for optical systems [2]. The fundamental difference, however, lies in the medium: while electronic ICs rely on the flow of electrons, PICs manipulate photons, the fundamental particles of light [2].

The significance of PICs cannot be overstated, particularly in the context of the modern digital age [1]. As the demand for high-speed data transmission and processing continues to grow exponentially, traditional electronic components face limitations due to issues like heat dissipation and signal interference [3]. PICs, leveraging the properties of light, offer a compelling solution to these challenges by enabling ultrafast data transmission with minimal energy loss and reduced heat generation [4]. Moreover, PICs can operate over a wide spectrum of frequencies, from the visible to the infrared range, making them highly versatile for a variety of applications [5].

1.1.2 Overview of Applications in Technology and Industry

The applications of Photonic Integrated Circuits span a broad range of industries, reflecting their versatility and potential to address some of the most pressing technological challenges today. In the telecommunications industry, PICs are at the forefront of revolutionizing optical fiber communications [6]. The integration of multiple optical functions on a single chip reduces the size, cost, and power consumption of the devices, making high-speed internet and data communication more accessible and efficient [7]. For instance, PICs are integral to the development of dense wavelength division multiplexing (DWDM) systems, which significantly increase the bandwidth of optical networks by allowing multiple data streams to be transmitted simultaneously on different wavelengths of light [8].

In the medical field, PICs are driving innovation in diagnostic equipment, partic-

ularly in areas like optical coherence tomography (OCT), a non-invasive imaging technique that provides high-resolution cross-sectional images of biological tissues [9]. The miniaturization and integration capabilities of PICs enable the development of portable, high-performance OCT devices, expanding their use in clinical settings and improving patient outcomes [10].
Environmental monitoring is another critical area where PICs are making significant contributions. Integrated photonic sensors are being developed to detect and measure various environmental parameters, such as air quality and water contamination, with high sensitivity and accuracy [11]. These sensors, owing to their compact size and low power requirements, can be deployed in remote and harsh environments, providing real-time data crucial for environmental protection and resource management [12].
Beyond these applications, PICs are also playing a pivotal role in emerging technologies such as quantum computing and LiDAR (Light Detection and Ranging) systems [13, 14]. In quantum computing, PICs are used to create scalable, stable platforms for manipulating quantum bits (qubits) with light, a key challenge in building practical quantum computers [15]. In LiDAR systems, which are essential for autonomous vehicles and 3D mapping, PICs offer a means to integrate the complex optical systems required for precise distance measurements onto a single chip, reducing costs and improving performance [16].
The continued development and deployment of PICs are expected to drive further innovation across these and other industries, underscoring their importance in the advancement of modern technology [1].

1.2 Motivation for the Research

1.2.1 The Need for Efficient Coupling Interfaces in PICs

While Photonic Integrated Circuits (PICs) hold the potential to revolutionize optical technologies by integrating multiple photonic components onto a single chip, a critical challenge remains in efficiently coupling these integrated components with external optical fibers [17]. The transition of optical signals between fibers and waveguides in PICs is particularly sensitive to coupling losses due to the significant mismatch in size and mode field diameter between the fiber core and the waveguide [5, 7].
A key focus of this research is the development and optimization of linear edge tapers as a coupling mechanism. Linear edge tapers have shown promise in mitigating these losses by gradually transitioning the mode field from the fiber to the waveguide, thereby improving the coupling efficiency [18]. Addressing these coupling inefficiencies is crucial, not only to enhance the performance of PICs but also to reduce energy consumption in data centers where optical interconnects are increasingly used to meet the demands of high-speed data transmission [14].
Furthermore, reducing coupling losses is essential in a variety of other applications, including telecommunications, where maintaining signal integrity is paramount, and in sensor networks, where low power consumption is critical [19]. The ability to efficiently couple light into PICs could lead to significant advancements in these

fields by enabling more compact, energy-efficient, and scalable optical systems [8]. This research aims to advance the design and implementation of linear edge tapers, optimizing them to achieve minimal coupling losses and demonstrating their potential across multiple high-impact applications. Such innovations are vital for the continued evolution of PIC technology and its broader adoption in commercial and industrial applications.

1.2.2 Challenges in Coupling Loss and Integration with Optical Fibers

One of the major challenges in the development of Photonic Integrated Circuits (PICs) is the efficient coupling of optical signals from standard optical fibers to nanophotonic waveguides. This challenge arises due to the significant size mismatch between typical single-mode optical fibers, which have a core diameter of around 9–10 µm, and the nanophotonic waveguides, which can have a cross-sectional size as small as 200–500 nm. This disparity leads to substantial coupling losses that degrade the overall performance of the system.

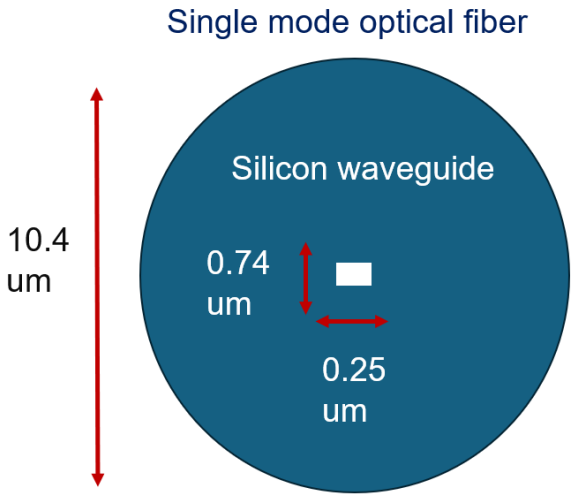

Figure 1.1: Illustration of the size mismatch between a standard single-mode optical fiber and a silicon nanophotonic waveguide. The difference in mode field diameters (MFD) results in significant coupling loss.

Coupling Efficiency Calculation: The coupling efficiency (η) between an optical fiber and a photonic waveguide is typically determined by the product of two terms: the Fresnel reflection efficiency (η_f) and the mode overlap efficiency (η_c) [25]:

$$\eta = \eta_f \times \eta_c \tag{1.1}$$

1. Fresnel Reflection Efficiency (η_f): This accounts for the reflection losses due to the difference in effective refractive indices between the optical fiber and the waveguide modes. The Fresnel efficiency is given by [25] :

$$\eta_F = \frac{4n_{\text{eff}}}{(1+n_{\text{eff}})^2} \tag{1.2}$$

For a typical silicon nanowire waveguide, with a refractive index of approximately 3.47 at a wavelength of 1.55 µm, and an optical fiber with a refractive index of 1.45, the Fresnel reflection efficiency can be around 79%.
2. Mode Overlap Efficiency (η_c): This term accounts for the overlap between the mode profiles of the optical fiber and the waveguide, defined as [25] :

$$\eta_c = \left| \frac{\iint_A E_{\text{fiber}}(x,y)\, E^*_{\text{wg}}(x,y)\, dx\, dy}{\sqrt{\iint_A |E_{\text{fiber}}(x,y)|^2\, dx\, dy}\sqrt{\iint_A |E_{\text{wg}}(x,y)|^2\, dx\, dy}} \right|^2 \tag{1.3}$$

Here, E_{fiber} and E_{wg} represent the electric field distributions in the fiber and waveguide, respectively. For highly confined modes in nanophotonic waveguides, the mode overlap efficiency can be as low as 0.006, leading to an overall coupling efficiency of less than 1%.
Tapered Waveguides to Mitigate Coupling Losses: One promising method to mitigate these coupling losses is through the use of linear edge tapers. By gradually reducing the width of the waveguide at the coupling interface, the effective mode field diameter can be increased, leading to better alignment with the optical fiber's mode. The length of the taper (L) must satisfy the adiabatic condition to ensure smooth mode conversion [7] :

$$L \gg z_b = \frac{2\pi}{|\beta^{(1)} - \beta^{(2)}|} \tag{1.4}$$

where z_b is the so-called beat length between modes with propagation constants $\beta^{(1)}$ and $\beta^{(2)}$. If the waveguide and taper cross-section are designed to support a single transverse mode, then $\beta^{(1)} = \beta^{\text{eff}}$ is the propagation constant of the mode at the fiber tip and $\beta^{(2)} = 2\pi n_{\text{cl}}/\lambda$ is the propagation constant of the radiation mode that is closest in value to the propagation constant of the guiding mode, with n_{cl} being the refractive index coefficient of the cladding.

1.3 Problem Statement and Research Questions

For this project, a linear edge taper was employed to address this issue in the lab. However, despite the theoretical advantages of using such tapers, significant optical coupling losses were recorded. Specifically, the losses measured approximately 1.5 dB when using a lensed fiber, which is considerably high for practical applications. This level of loss can drastically affect the overall performance of photonic systems, making it essential to investigate the underlying causes.
The master project focuses on identifying the potential factors contributing to these significant coupling losses. Several key elements are hypothesized to influence the efficiency of the coupling interface, including:

- **Taper dimensions:** Could the geometry of the taper be inadequately optimized, leading to a mismatch with the fiber mode?
- **Taper gap:** Is there a misalignment or spacing issue between the taper and fiber that contributes to the loss?
- **SiO2 thickness levels:** Could the thickness of the silicon dioxide cladding layer be impacting the optical mode confinement?

- **Sidewall roughness and defects:** Are the imperfections in the fabricated taper sidewalls causing scattering losses?
- **Fiber choice:** Would using a standard single-mode fiber (SMF) instead of a lensed fiber result in better coupling efficiency?

The SEM images below taken by Vijay Shekhawat in the MC2 cleanroom facility, provide a top-down view of the fabricated linear edge taper. These images highlight potential issues such as sidewall roughness and taper geometry, which are central to this investigation.

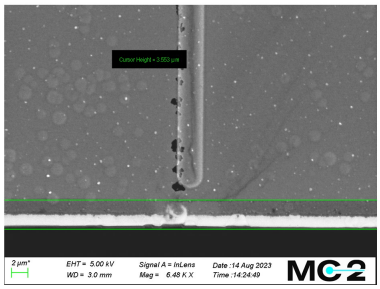

Figure 1.2: Top view SEM image of the linear edge taper used in the lab.

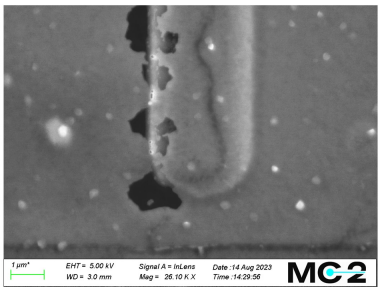

Figure 1.3: Closer SEM image, focusing on the sidewall roughness.

1.3.1 Objectives of the Study

The primary objective of this research is to investigate the underlying causes of the relatively high coupling losses observed in the linear edge taper structure.
To address this issue, the project will utilize electromagnetic (EM) solver software to model and simulate the taper structure, aiming to understand the factors contributing to the coupling inefficiencies.
The key goals of the study are as follows:

- Analyze the performance of the current linear edge taper design to identify sources of coupling loss, including taper geometry, SiO2 thickness, and taper gap effect.
- Simulate the optical coupling interface using advanced EM solvers to assess how different design parameters impact coupling efficiency.
- Propose optimized designs that could reduce the coupling losses further.
- Validate the proposed solutions through simulations and, where possible, experiments to demonstrate the improved performance of the taper structure.

The successful reduction of coupling losses would mark a significant improvement in the performance of PICs and would open the door to more energy-efficient and scalable optical systems for applications ranging from telecommunications to sensor networks.

2

Literature Review

Efficient coupling of light between optical fibers and photonic waveguides is crucial for minimizing insertion losses in photonic integrated circuits (PICs). Two common methods for achieving this coupling are grating couplers and edge couplers. This chapter provides an in-depth review of these coupling techniques, detailing their operating principles, advantages, limitations, and the key equations that describe their performance.

2.1 Grating Couplers

2.1.1 Concept and Operation

Grating couplers enable efficient coupling of light from an optical fiber into a waveguide by utilizing periodic structures that diffract light at specific angles. Typically, the optical fiber is positioned at an angle relative to the waveguide to maximize coupling efficiency. The operation of grating couplers is governed by the grating equation, which matches the momentum of the guided mode with that of the incident light:

$$k_0 n_{\text{cl}} \sin\theta = \beta - \frac{2\pi m}{\Lambda} \tag{2.1}$$

where:

- k_0 is the free-space wave number,
- n_{cl} is the refractive index of the cladding,
- θ is the incident angle from the fiber,
- β is the propagation constant of the waveguide mode,
- m is the diffraction order (an integer),
- Λ is the grating period.

The principle behind grating couplers is to satisfy this momentum-matching condition to efficiently diffract light from the fiber into the waveguide [20]. The coupling efficiency is highly dependent on the design parameters of the grating, such as the period, depth, and incident angle.

2.1.2 Coupling Efficiency

The total coupling efficiency (η_{gc}) of a grating coupler is influenced by several factors, including scattering, directionality, and mode overlap. It can be expressed as [7] :

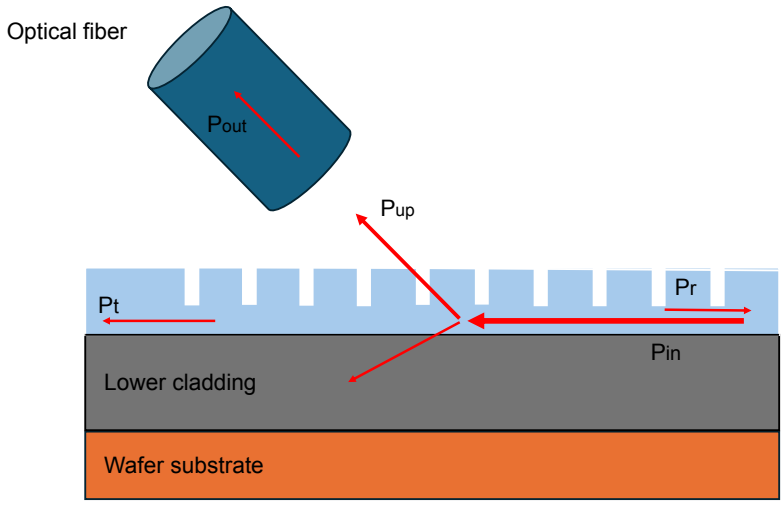

Figure 2.1: Diagram of a grating coupler showing light coupling from an optical fiber into a waveguide using a periodic grating structure.

$$\eta_{\text{gc}} = \eta_{\text{s}}\eta_{\text{d}}\eta_{\text{c}} \tag{2.2}$$

where:

- η_{s} is the scattering efficiency,
- η_{d} is the directionality,
- η_{c} is the mode overlap efficiency.

These parameters have been verified both experimentally and theoretically in several studies [21, 22], demonstrating that the efficiency of grating couplers depends on the careful design of the grating parameters and precise alignment with the optical fiber. The scattering efficiency (η_{s}) is calculated as:

$$\eta_{\text{s}} = \frac{P_{\text{in}} - P_{\text{t}} - P_{\text{r}}}{P_{\text{in}}} \tag{2.3}$$

where:

- P_{in} is the total input power,
- P_{t} is the power transmitted through the waveguide,
- P_{r} is the reflected power.

The directionality (η_{d}) quantifies the amount of light coupled into the waveguide relative to the power radiated upwards and is given by:

$$\eta_{\text{d}} = \frac{P_{\text{up}}}{P_{\text{up}} + P_{\text{down}}} \tag{2.4}$$

where:

- P_{up} is the power radiated upwards (towards the fiber),
- P_{down} is the power radiated downwards into the substrate.

The mode overlap efficiency (η_{c}) measures how well the optical mode in the fiber overlaps with the mode in the waveguide and is defined as:

$$\eta_c = \frac{\left| \int E^{(\mathrm{up})} E^{(\mathrm{out})^*} dA \right|^2}{\left(\int \left| E^{(\mathrm{up})} \right|^2 dA \right) \left(\int \left| E^{(\mathrm{out})} \right|^2 dA \right)} \tag{2.5}$$

where:

- $E^{(\mathrm{up})}$ is the electric field of the mode radiated upwards from the waveguide,
- $E^{(\mathrm{out})}$ is the electric field of the outgoing mode in the waveguide,
- dA is the differential area element.

2.1.3 Advantages of Grating Couplers

Grating couplers offer several advantages in integrated photonic systems due to their simplicity and ease of integration [20]. Firstly, they are relatively easy to fabricate using standard lithography techniques, making them highly compatible with existing CMOS fabrication infrastructure. Secondly, grating couplers allow for vertical fiber-to-chip coupling, which simplifies wafer-level testing. Lastly, they offer scalability, as grating couplers can be placed at multiple locations on the same chip, facilitating multiple optical interfaces for complex PIC designs.

2.1.4 Limitations of Grating Couplers

Despite their advantages, grating couplers have certain limitations that can restrict their applicability in some scenarios [17, 7]. One major limitation is their narrow bandwidth; grating couplers typically have a limited operational bandwidth of a few tens of nanometers, making them unsuitable for broadband applications or scenarios requiring a wide wavelength range [17]. This limitation arises due to the wavelength-dependent diffraction condition of the grating structure.

Additionally, grating couplers often exhibit higher insertion losses compared to edge couplers, typically ranging between 1 and 3 dB [20]. This level of loss can be problematic for systems where minimizing losses is critical. Grating couplers are also highly sensitive to the angle of incidence from the fiber, requiring precise alignment during assembly to achieve optimal coupling efficiency, which can complicate packaging and increase costs [7]. Moreover, they can exhibit polarization-dependent loss due to their anisotropic diffraction properties, necessitating polarization management techniques in the system design [7]. Finally, the periodic structure of grating couplers can cause back-reflections into the fiber, potentially interfering with sensitive components like lasers and detectors [17].

These limitations make grating couplers less suitable for applications requiring broad bandwidth, extremely low insertion losses, or robust alignment tolerances. Therefore, alternative coupling methods, such as edge couplers, may be preferred in such scenarios.

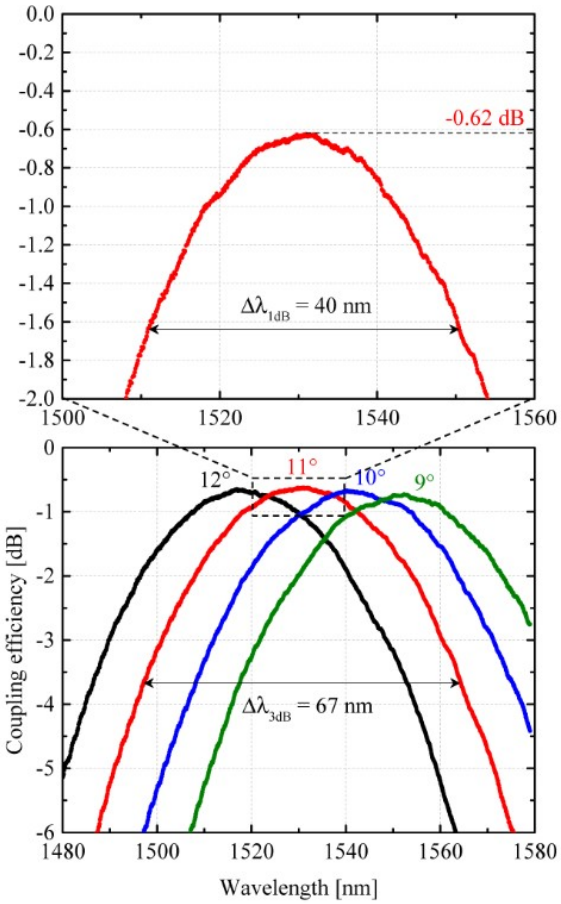

Figure 2.2: Spectral response of a typical grating coupler, showing limited bandwidth. Reproduced from [17] under the Creative Commons CC BY 3.0 license.

2.2 Edge Couplers

2.2.1 Concept and Operation

Edge couplers, also known as butt couplers facilitate the coupling of light between an optical fiber and an on-chip waveguide by aligning the fiber to the edge of the chip. Unlike grating couplers, which couple light vertically via diffraction gratings, edge couplers transfer light horizontally through the cleaved facet of the chip. The primary principle behind edge couplers is the adiabatic transition of the optical mode from the fiber to the waveguide, achieved by tapering the waveguide dimensions to match the mode field diameter (MFD) of the fiber [23].

The fundamental concept relies on maximizing the mode overlap between the fiber mode and the waveguide mode at the interface. By gradually tapering the waveguide from a wider dimension—matching the fiber MFD—to the standard waveguide dimensions used for on-chip propagation, efficient coupling can be achieved with minimal reflection and scattering losses.

The total coupling efficiency (η) between an optical fiber and a photonic waveguide is determined by the product of the Fresnel reflection efficiency (η_f) and the mode overlap efficiency (η_c) as mentioned earlier in eq (1.1 to 1.3).

Hence , optimizing the taper geometry and managing the refractive index contrast are crucial steps in enhancing η_c and η_f, respectively. In practical designs, reducing the refractive index mismatch at the interface—such as by using intermediate layers or optimizing the waveguide dimensions—can improve η_f. Simultaneously, tailoring the taper profile to expand or contract the mode field diameter helps maximize η_c by ensuring better overlap between the fiber and waveguide modes. When the waveguide narrows to subwavelength dimensions at the facet, the optical mode expands into the cladding, increasing the overlap with the fiber mode.
By carefully considering both the Fresnel reflection and mode overlap efficiencies, edge couplers can be designed to achieve high overall coupling efficiency.

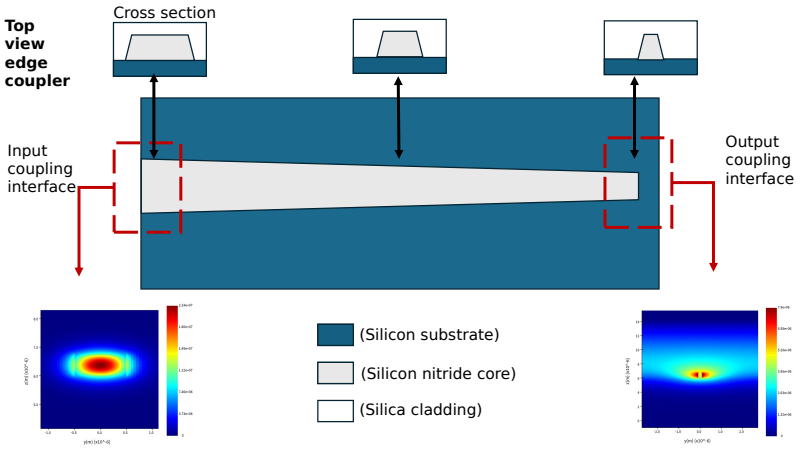

Figure 2.3: Diagram of an edge coupler showing light coupling from an optical fiber into a waveguide via an edge interface with a tapered waveguide.

2.2.2 Advantages of Edge Couplers

Edge couplers offer several advantages over grating couplers, particularly in applications requiring high bandwidth and low losses [7]. One of the primary advantages is their broad bandwidth; edge couplers provide a wide operational bandwidth, often exceeding 100 nm, making them suitable for broadband applications and wavelength-division multiplexing systems. Additionally, with careful design, edge couplers can achieve ultralow coupling losses, sometimes less than 1 dB, which is critical in systems where minimizing loss is essential [21]. They also offer high coupling efficiency due to efficient mode overlap between the fiber and the expanded waveguide mode. Moreover, edge couplers can be designed to be relatively insensitive to polarization compared to grating couplers, reducing the need for polarization management [7].
In this research, edge couplers were chosen due to their wider bandwidth and the potential to achieve ultralow coupling losses, which are essential for high-performance photonic integrated circuits.

2.2.3 Limitations of Edge Couplers

Despite their advantages, edge couplers have certain limitations [23, 7]. Fabrication complexity is one of the main challenges; creating the inverse taper requires

high-precision fabrication techniques to achieve the subwavelength dimensions and smooth sidewalls necessary for low-loss operation. Assembly can also be challenging, as precise alignment between the fiber and the chip facet is necessary, which can complicate packaging and increase costs. Additionally, edge coupling necessitates a high-quality cleaved or polished facet, which may not be compatible with all fabrication processes or materials.

3
Methodology

3.1 Introduction

Simulation plays a crucial role in the design and optimization of photonic devices, allowing for the analysis of complex structures before fabrication. In this chapter, we discuss the simulation methods employed in this thesis work: the Finite Difference Eigenmode (FDE) method, the Eigenmode Expansion (EME) method, and the Finite Difference Time Domain (FDTD) method. Each of these methods offers unique advantages and limitations, which we explore in the context of simulating optical coupling in photonic integrated circuits (PICs).
Efficient coupling between optical fibers and silicon nitride (Si3N4) waveguides is critical for the performance of PICs. A linear edge taper was employed to facilitate this coupling, however coupling losses of approximately **1.1 dB** were observed with lensed fibers in our experimental measurements. These losses may be attributed as identified in section 1.3 to various factors such as taper geometry, cladding thickness, sidewall roughness, physical and taper gaps . Addressing these challenges requires a systematic analysis of how each parameter impacts coupling efficiency.
Simulations were performed using the **Finite-Difference Eigenmode (FDE)**, **Eigenmode Expansion (EME)**, and **Finite-Difference Time-Domain (FDTD)** methods to optimize the edge taper design and analyze the effects of geometric and material parameters where figure 3.1 illustrates the simulation setup, highlighting the key variables investigated.

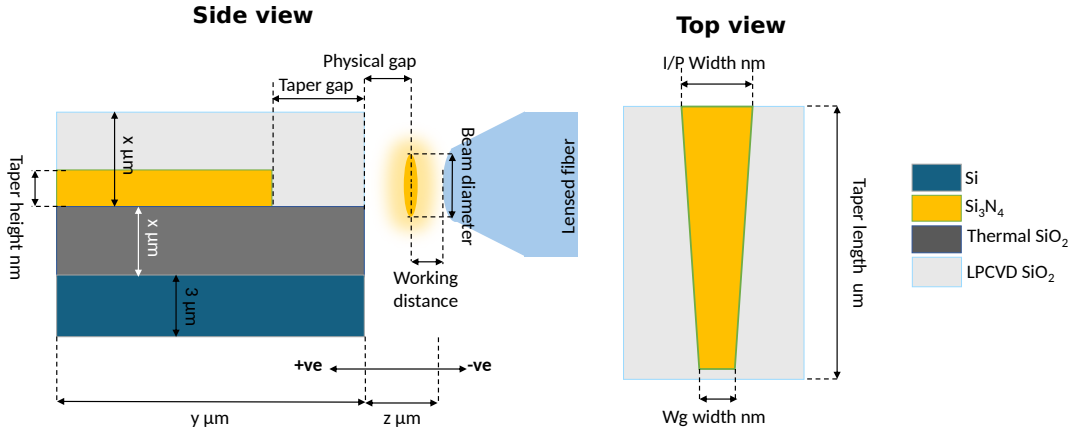

Figure 3.1: Schematic of the linear edge coupler simulation setup, showing key parameters such as taper dimensions, cladding thickness, and fiber alignment gaps.

3.2 Simulation Setup and Methods

The simulation setup for the linear adiabatic edge coupler in fig 3.1 was implemented using the Ansys Lumerical software suite. The setup involved modeling the waveguide taper geometry, material properties, and boundary conditions to accurately simulate the coupling between the optical fiber and the nanophotonic waveguide.
The waveguide geometry consisted of a linear taper with a starting width matching the fiber mode field diameter and tapering down to the standard waveguide width. Silicon nitride (Si3N4) was used for the waveguide core, and silicon dioxide (SiO2) served as the cladding layers. Perfectly matched layers (PML) were employed as boundary conditions to absorb outgoing waves and prevent reflections at the simulation domain boundaries. A fine mesh was applied in regions with high field variations to ensure accurate results. The source was defined as a Gaussian beam representing the optical fiber, placed at the input facet of the taper.
Different numerical methods were used to analyze specific aspects of the system:

- **FDE method**: Calculated mode profiles and effective indices of the waveguide and fiber modes, estimating mode mismatch losses.
- **EME method**: Simulated taper lengths to ensure adiabatic mode transformation while balancing device footprint and efficiency.
- **FDTD method**: Simulated full 3D electromagnetic interactions, assessing the effects of taper facet width, cladding thickness, and alignment gaps.

Each method was chosen to complement the others, providing both preliminary insights and detailed analyses.

3.3 Simulation Methods

3.3.1 Finite Difference Eigenmode (FDE) Method Concept

The Finite Difference Eigenmode (FDE) method is a numerical technique used to calculate the eigenmodes of waveguides by solving Maxwell's equations in the frequency domain [24]. The FDE method discretizes the cross-sectional area of the waveguide using a finite difference grid, transforming the continuous differential equations into a matrix eigenvalue problem. This method allows for the determination of the effective indices and field profiles of the guided modes.
The FDE method solves the following eigenvalue equation for the transverse electric field $\mathbf{E}_t$:

$$\nabla_t \times \left(\frac{1}{\mu} \nabla_t \times \mathbf{E}_t \right) - k_0^2 \varepsilon_r \mathbf{E}_t = \beta^2 \mathbf{E}_t, \tag{3.1}$$

where:

- ∇_t is the transverse gradient operator,
- μ is the permeability,
- k_0 is the free-space wave number,
- ε_r is the relative permittivity,
- β is the propagation constant.

By solving Eq. (3.1), the effective indices $n_{\text{eff}} = \beta/k_0$ and corresponding mode profiles are obtained.

3.3.1.1 Application in the Study

In this research, the FDE method was employed to obtain a preliminary understanding of the coupling losses resulting from direct butt coupling between a standard single-mode fiber (SMF) or lensed fiber and the nanophotonic waveguide. The analysis focused on quantifying the mode mismatch losses due to the disparity in mode field diameters (MFD) between the fiber and the waveguide [25].
The FDE simulations provided the mode profiles of the fiber and waveguide separately.
However, the FDE method in this context does not account for Fresnel reflections at the interface between the fiber and the waveguide, as it considers only the transverse modes and assumes perfect modal matching [25]. Therefore, the calculated coupling losses represent only the losses due to mode size mismatch.

3.3.1.2 Limitations

While the FDE method is efficient for calculating mode profiles and effective indices, it has limitations:

- It is inherently a 2D simulation, considering only the cross-sectional plane of the waveguide.
- It does not account for longitudinal variations. Although it generally ignores Fresnel reflections, these can only be indirectly accounted for by considering the effective index mismatch between the modes of interest.
- It assumes uniform structures along the propagation direction.

Due to these limitations, the FDE method provides an initial estimation but is insufficient for accurately predicting the total coupling losses in the system.

3.3.2 Eigenmode Expansion (EME) Method

3.3.2.1 Application in the Study

In this project, the EME method was utilized to estimate the appropriate length of the inverse taper in the edge coupler design. The goal was to ensure that the adiabatic condition is met, allowing for efficient mode transformation from the expanded mode at the facet to the confined mode in the nanophotonic waveguide [26].
The EME simulations provided the S-parameters, particularly the transmission coefficient S_{21}, which represents the power transmitted from port 1 (input) to port 2 (output). By analyzing the magnitude of $|S_{21}|^2$, the optimal taper length L was determined to maximize coupling efficiency.
The adiabatic condition requires that the taper length satisfies Eq.(1.4) [26]:
By simulating different taper lengths and geometries, the EME method allowed for the optimization of the taper design to achieve efficient coupling.

3.3.2.2 Advantages

The EME method offers several advantages: It efficiently models structures with longitudinal variations. additionally it accurately accounts for mode coupling and reflections at interfaces. another merit is that it provides S-parameters, which are essential for analyzing the performance of photonic components. Finally EME method is computationally less intensive than full 3D simulations for certain structures.
However, the EME method may face challenges with structures exhibiting rapid variations or requiring high-resolution in all three dimensions.

3.3.3 Finite Difference Time Domain (FDTD) Method

3.3.3.1 Application in the Study

In this research, the FDTD method was employed to perform comprehensive 3D simulations of the coupling between the SMF/lensed fiber and the nanophotonic waveguide. High-resolution mesh settings were used to accurately capture the electromagnetic interactions at the interface. The FDTD simulations accounted for both: **Fresnel Reflections**: which is caused by the refractive index contrast at the interface between the fiber and the waveguide and the **Mode Field Diameter (MFD) Mismatch** which happens due to the disparity in mode sizes between the fiber and the waveguide modes.
By solving Maxwell's equations in the time domain, the FDTD method provided detailed insights into the coupling losses and allowed for the visualization of field distributions and scattering effects [27].

3.3.3.2 Advantages

The FDTD method offers several advantages:

- It provides full-wave solutions, accurately modeling complex electromagnetic interactions.
- It can simulate broadband responses in a single run.
- It captures both near-field and far-field effects.
- It handles arbitrary geometries and material properties [28].

However, the FDTD method is computationally intensive, especially for 3D simulations with fine mesh resolutions. It requires significant computational resources and time, particularly for structures with large dimensions relative to the wavelength.

3.4 Simulation Workflow

3.4.1 Initial Analysis with FDE

The initial step involved using the FDE method to calculate the mode profiles and effective indices of both the fiber and the nanophotonic waveguide. This provided insights into the fundamental mode properties and allowed for the estimation of coupling efficiency due to mode overlap.

3.4.2 Taper Optimization with EME

Following the initial analysis, the EME method was employed to design and optimize the inverse taper of the edge coupler. By simulating various taper lengths and profiles, the optimal geometry that satisfies the adiabatic condition was determined, maximizing the coupling efficiency between the fiber and the waveguide.

3.4.3 Comprehensive Analysis with FDTD

The final step involved using the FDTD method for a full 3D simulation of the optimized taper structure. This comprehensive analysis accounted for all electromagnetic interactions, including reflections and scattering, providing an accurate assessment of the overall coupling performance.

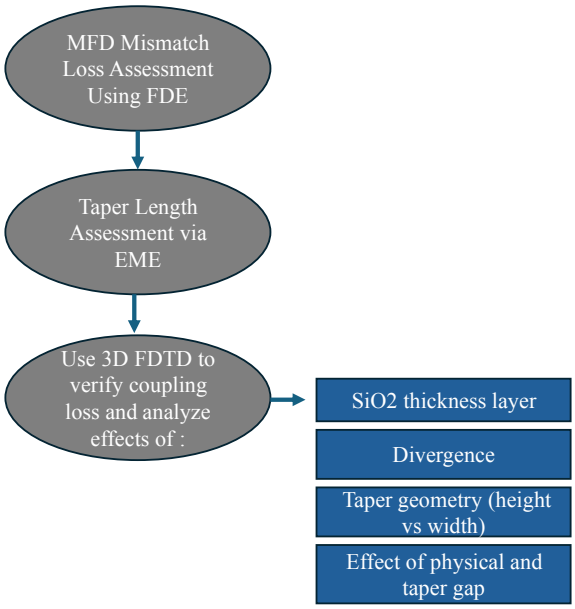

Figure 3.2: Simulation workflow illustrating the sequential use of FDE, EME, and FDTD methods for optimizing coupling interfaces in PICs.

3.4.4 Waveguide Material and Geometry

Silicon nitride (Si3N4) was selected as the core material for the nanophotonic waveguide due to its low optical loss at telecommunications wavelengths, wide transparency window ranging from the visible to the mid-infrared spectrum, compatibility with standard CMOS fabrication processes, excellent thermal stability with a moderate thermo-optic coefficient, and lattice compatibility with silicon dioxide (SiO2), which minimizes interface defects and scattering losses.
The waveguide geometry consisted of a linear edge taper, where the width of the waveguide gradually reduces along the direction of propagation. The taper started with a width matching the fiber mode field diameter and narrowed down to the standard waveguide width required for on-chip propagation. The taper length and

profile were optimized using the EME method to satisfy the adiabatic condition and minimize coupling losses.

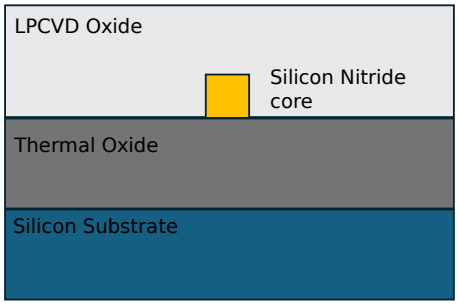

Figure 3.3: Cross-sectional view of the silicon nitride waveguide.

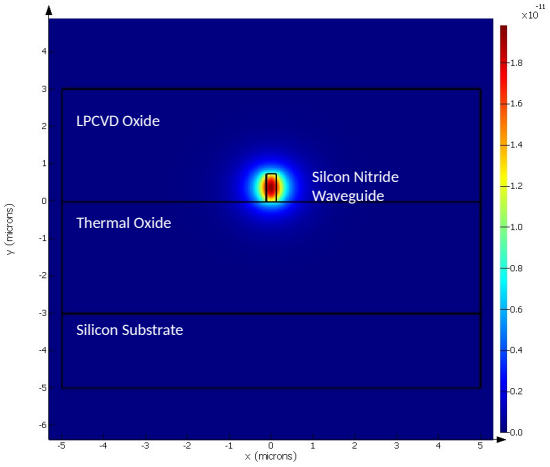

Figure 3.4: Cross-sectional profile of the TE mode at the taper facet.

The taper height was consistently set to 740nm (except during parameter sweeps) because this height was found to be optimal for achieving anomalous dispersion in the waveguide, which is important for phase matching in Kerr nonlinear optics. Additionally, this height is achievable with the existing cleanroom nanofabrication techniques in the MC2 cleanroom facility, ensuring that the designed structures can be reliably fabricated.
The cladding material consisted of two layers of silicon dioxide (SiO2). The lower cladding was a thermally grown SiO2 layer providing a high-quality interface with the silicon substrate, while the upper cladding was a layer of low-pressure chemical vapor deposition (LPCVD) SiO2 serving to protect the waveguide and provide optical confinement [18] .

3.4.5 Fiber Structures Examined

3.4.5.1 Lensed Fiber

A lensed fiber model with a beam waist radius of 1.25 µm was considered, reflecting the lab setup where a lensed fiber was used for coupling. The lensed fiber focuses

the light to a smaller spot size, enhancing coupling efficiency with the nanophotonic waveguide. In the EME and FDTD simulations, the lensed fiber was modeled as a Gaussian source with a beam waist radius of 1.25 µm placed opposite the edge taper facet. This approximation effectively represents the lensed fiber in coupling simulations, considering the reciprocity of the passive taper device (i.e., $|S_{21}| = |S_{12}|$).

3.4.5.2 Standard Single-Mode Fiber (SMF)

A standard single-mode fiber (SMF) was also analyzed to evaluate the coupling losses. The SMF had a core diameter of 10 µm, corresponding to a mode field diameter of approximately 10.4 µm at 1550 nm, and a cladding diameter of 125 µm. The core material was doped silica, and the cladding was pure silica.

In the FDE simulations, the SMF was modeled by setting the beam waist radius to match that of the SMF mode field diameter, as the FDE method considers cross-sectional mode profiles. In the EME and FDTD simulations, the SMF was modeled with its actual cylindrical geometry, including the core and cladding, accurately representing the fiber geometry.

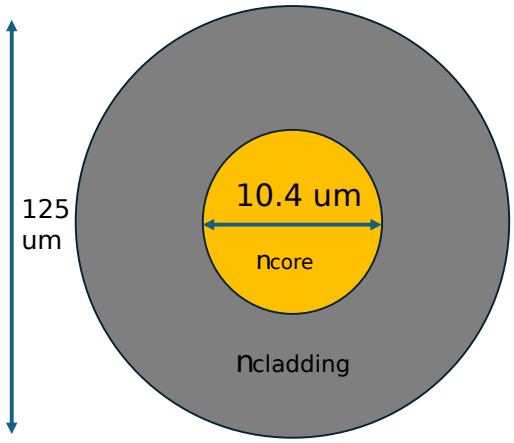

Figure 3.5: Cross-sectional view of the standard single-mode fiber (SMF).

3.5 Modeling Approaches

3.5.1 Lensed Fiber Modeling

In the EME and FDTD simulations, the lensed fiber was represented as a Gaussian beam source with a beam waist radius of 1.25 micrometer. This approach is justified because the lensed fiber focuses light into a small spot, and the Gaussian beam approximation effectively captures the mode profile for coupling analysis [29]. The source was placed opposite the edge taper facet, and reciprocity was assumed for the passive taper structure, allowing for accurate coupling efficiency calculations.

3.5.2 SMF Modeling

For the SMF, different modeling strategies were employed based on the simulation method. In the FDE simulations, the SMF was modeled by setting the beam waist radius to match the mode field diameter of the SMF, suitable for cross-sectional simulations focusing on mode overlap. In the EME and FDTD simulations, the SMF was modeled with its actual cylindrical geometry, including the core and cladding. This detailed representation allows for accurate simulation of the coupling process, including effects such as Fresnel reflections and modal dispersion.

3.6 Taper Geometry and Dimensions

The taper geometry was a linear edge taper, where the waveguide width gradually decreases along the propagation direction. It started with a width matching the fiber mode field diameter and narrowed down to the standard waveguide width required for on-chip propagation. The taper length and profile were optimized using the EME method to satisfy the adiabatic condition and minimize coupling losses.
The taper height was consistently set to 740nm (except during parameter sweeps) because this height was found optimal for combating anomalous dispersion in the waveguide, which is important for maintaining signal integrity and minimizing pulse broadening. Additionally, this height is achievable with existing cleanroom nanofabrication techniques, ensuring that the designed structures can be reliably fabricated.
We also include a figure showing the constructed Si3N4 linear taper in the simulation environment, where X_1 represents the width at the input facet, X_2 represents the width at the taper edge, and Y represents the constant height of the taper structure (Figure 3.6).

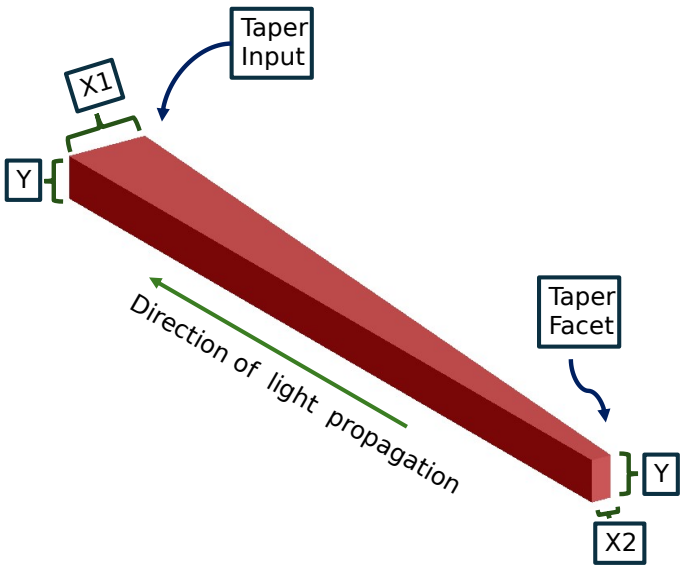

Figure 3.6: Schematic of the Si3N4 linear taper in the simulation environment, where X_1 represents the width at the input facet, X_2 represents the width at the taper edge, and Y represents the constant height of the taper structure.

3.7 Simulation Parameters Summary

Table 3.1: Summary of simulation parameters and variables.

Parameter	**Value**
Central Wavelength (λ)	1550 nm
Waveguide Core Material	Silicon Nitride (Si_3N_4)
Waveguide Core Refractive Index	$n = 1.991$ at 1550 nm
Waveguide Cladding Material	Two layers: Upper LPCVD SiO_2, Lower Thermal SiO_2
Upper Cladding Refractive Index	$n = 1.44385$
Lower Cladding Refractive Index	$n = 1.4431$
Waveguide Height	740 nm
Lensed Fiber Beam Waist Radius	1.25 μm
SMF Core Diameter	10.4 μm
SMF Cladding Diameter	125 μm
Refractive Index of SMF Core	$n \approx 1.45$
Refractive Index of SMF Cladding	$n = 1.44$

4

Results and Discussion

4.1 Introduction

This chapter presents a comprehensive analysis of the simulation results aimed at optimizing the coupling efficiency between an adiabatic linear silicon nitride (Si3N4) taper and optical fibers, specifically single-mode fibers (SMF-28) and lensed fibers. Simulations were conducted using Ansys Lumerical software, employing both Finite-Difference Time-Domain (FDTD) and Eigenmode Expansion (EME) methods to evaluate the optical behavior at the coupling interface.

The study began with preliminary simulations using the Finite-Difference Eigenmode (FDE) solver to gain insights into the mode field diameter (MFD) matching between the taper structure and the fiber modes of both SMF and lensed fibers. This initial analysis established an optimal taper facet width range that minimizes coupling loss due to MFD mismatch. Based on these preliminary results, a more detailed analysis was conducted using the EME solver to determine the optimal taper length for maximal electromagnetic transmission through the adiabatic structure. Following the EME simulations, the FDTD solver was implemented to analyze various effects including the impact of taper dimensions, silica cladding thickness, physical gaps introduced between the edge of the taper face and the fiber, and the effect of beam divergence.

4.2 Optimal Taper Length Determination via EME Simulation and Experimental Validation

Using the EME solver in Ansys, the optimal taper length was investigated for a taper facet geometry of 740 nm height and 200 nm width, selected based on low-loss configurations identified in the preliminary FDE simulations.

For coupling to a lensed fiber (as depicted in figure 4.1) the EME results indicate that a taper length of 50 µm achieves nearly 95 percenatage of tranmsission while still keeping a relatively small footprint optical power transfer, with $|S_{21}|^2$ close to 0.95.

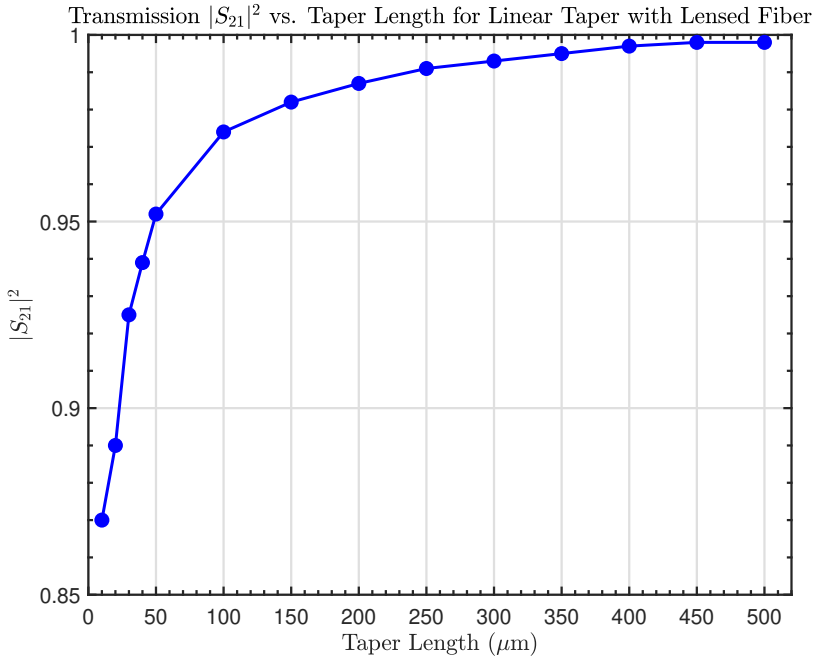

Figure 4.1: Transmission $|S_{21}|^2$ vs. taper length for linear taper coupled with lensed fiber

This shorter taper length allows for a compact design suitable for fabrication, ensuring efficient power transmission without excessive footprint. For SMF coupling, however, the optimal taper length is approximately 1 mm, as seen in Figure 4.2.

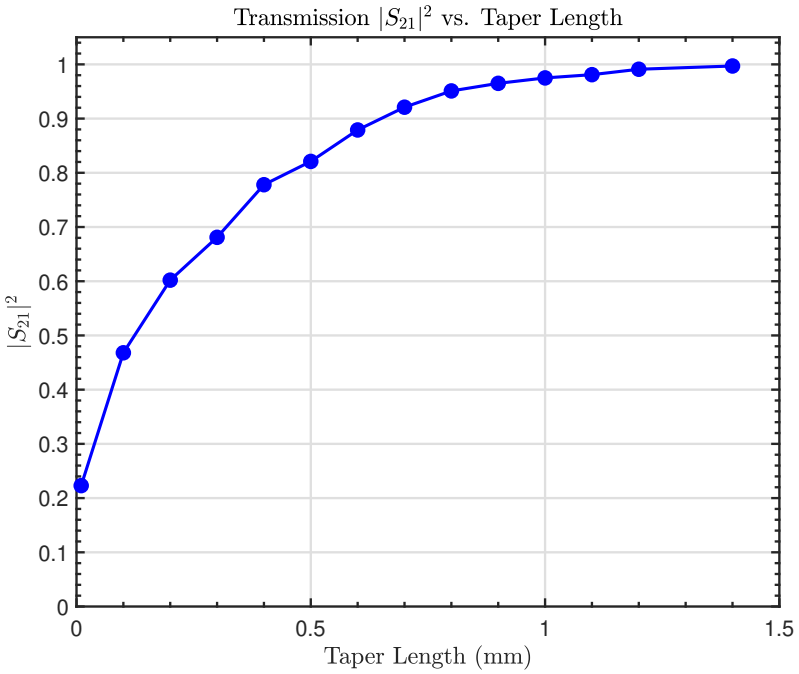

Figure 4.2: Transmission $|S_{21}|^2$ vs. taper length for linear taper coupled with SMF

This longer taper length is necessary to accommodate the mode field diameter (MFD) difference and maintain mode stability over a greater distance, achieving a nearly complete transfer of energy.

4.2.1 Experimental Validation of Taper Length for Lensed Fiber

To validate the simulation results, a prototype of the linear taper developed in our simulations was fabricated in a cleanroom environment. The taper geometry closely resembled the configuration used in the simulation setup as depicted in fig (3.1), with a waveguide made of silicon nitride (Si3N4) and cladding layers of both LPCVD and thermal silicon dioxide (SiO2) each with a thickness of **3 µm**. The taper gap (the distance from the taper facet to the chip edge) was fixed at **0.25 µm**, limited by fabrication constraints with the taper facet being **740 nm** high and **250 nm** wide. A lensed fiber with a beam waist diameter of **2.5 µm** was employed to couple light into the taper. The fiber was aligned with minimal physical separation to the taper facet to maximize coupling efficiency. A laser with a central wavelength of **1550 nm** and an output power of **-1.5 dBm** was used to test the coupling efficiency.
The experimental setup was designed to measure both the coupling loss per facet and the overall insertion loss (fiber-to-chip-to-fiber). The experimental results are presented in Figure 4.3, showing the coupling loss and insertion loss as a function of taper length.

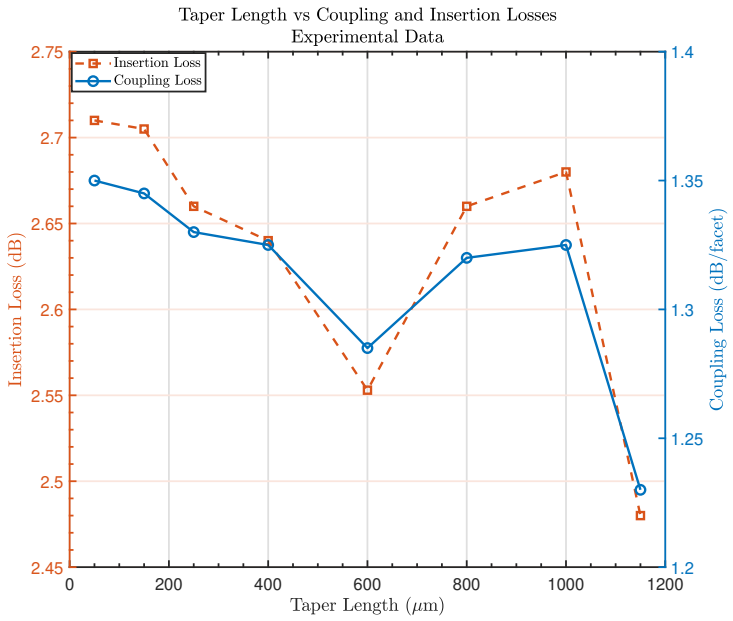

Figure 4.3: Experimental coupling loss and insertion loss vs. taper length for the fabricated prototype. The measurements were conducted by my supervisor Vijay Shekhawat. All subsequent experimental results presented in this thesis are based on tests performed by Vijay Shekhawat, a PhD student in the group.

The experimental results indicate that the coupling loss varies minimally (around **0.1 dB** across the taper lengths), while the insertion loss shows a difference of approximately **0.4 dB** between the maximum and minimum recorded values. Notably, the experimental data supports the simulation prediction that a taper length of **50 µm** yields nearly optimal transmission efficiency relative to the size of the device. Although the lowest coupling and insertion losses were observed at a taper length of **1.2 mm**, this comes at the expense of a larger device footprint.
The coupling loss does not decrease monotonically with increasing taper length. This non-monotonic behavior can be attributed to the interplay between taper length and practical fabrication imperfections. While longer tapers theoretically allow for more gradual mode evolution, making the mode transformation more adiabatic and reducing reflections, in practice, other loss mechanisms become significant. As the taper length increases, the cumulative effect of scattering losses due to sidewall roughness and fabrication-induced defects along the taper also increases. These scattering losses can offset the benefits gained from a more adiabatic taper, resulting in minimal net improvement or even slight increases in coupling loss for longer tapers.
The discrepancy between simulations and measurements may be explained by considering the idealized conditions assumed in simulations versus the realities of experimental implementations. Simulations assume perfect material properties, exact geometries, and ideal alignments, neglecting fabrication tolerances and imperfections. In the fabricated prototypes, factors such as sidewall roughness, variations in taper width and height, and deviations in refractive indices due to material deposition processes can introduce additional losses not accounted for in simulations.
Furthermore, alignment errors during experimental setup can contribute to discrepancies. Precise alignment is critical for optimal coupling efficiency, and slight misalignments in lateral or angular positioning of the lensed fiber can reduce mode overlap and increase losses. The lensed fiber's actual beam profile may also deviate from the ideal Gaussian profile used in simulations due to manufacturing tolerances of the fiber tip, leading to further differences between simulated and measured results.
The combination of fabrication imperfections, fixed taper gap, beam divergence, and alignment challenges may explain both the non-monotonic trend in coupling loss with taper length and the discrepancy between simulations and experimental measurements.

4.2.2 Mode Profiles of Optimal Taper Configurations

The mode profiles in both the XY and XZ planes were evaluated for the optimized taper configurations for SMF and lensed fiber couplings as depicted in figure 4.4. The following figure presents a combined view of the XY and XZ mode propagation profiles for both fiber types.
As the taper geometry narrows toward the facet, the fundamental TE mode in the SMF configuration begins to expand, attempting to match the MFD of the fiber. This "blow-up" effect observed in the mode field is due to the mode's adaptation to the decreasing cross-sectional area, which allows for a gradual transition from the confined taper mode to the fiber mode.

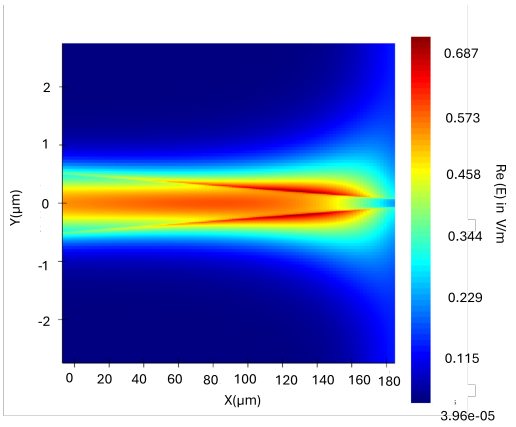

(a) XY profile for SMF coupling (125 nm taper width)

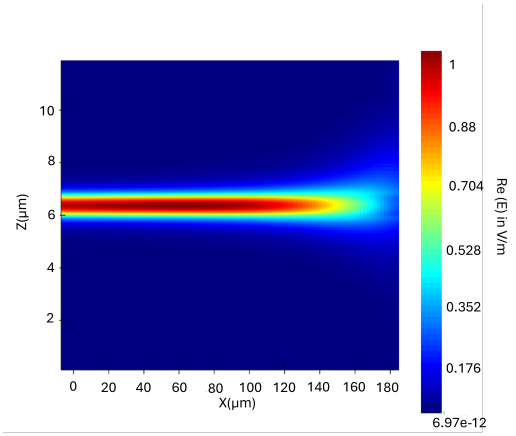

(b) XZ profile for SMF coupling (125 nm taper width)

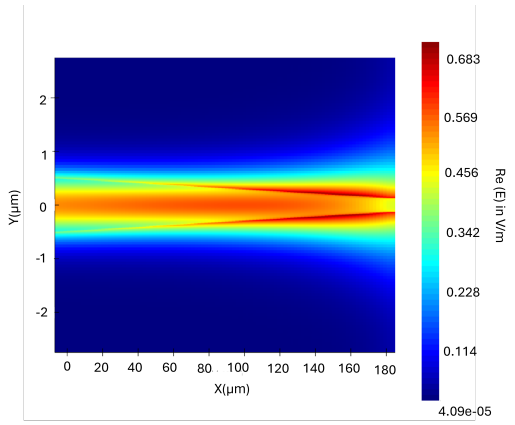

(c) XY profile for lensed fiber coupling (250 nm taper width)

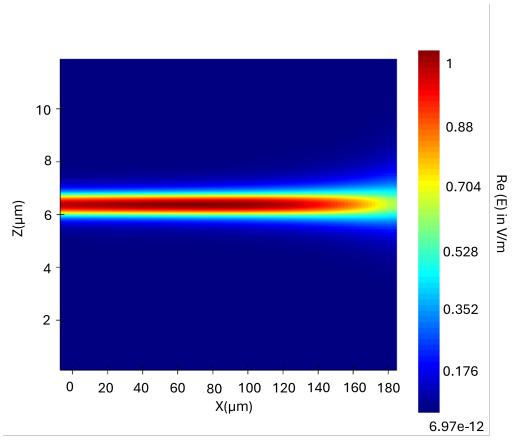

(d) XZ profile for lensed fiber coupling (250 nm taper width)

Figure 4.4: Combined mode profiles for SMF and lensed fiber coupling. (a) and (b) show the XY and XZ profiles for SMF coupling, respectively. (c) and (d) depict the XY and XZ profiles for lensed fiber coupling. These plots illustrate field expansion and confinement characteristics for each configuration along the taper length where the bar charts depicts the magnitude of the E-field in the taper structure while the X, Y and Z dimensions are expressed in micrometers.

For the lensed fiber coupling, the mode profile at a 250 nm width aligns efficiently with the lensed fiber's 2.5 µm beam waist, minimizing reflection losses and enhancing overlap.

4.3 Effect of Taper Dimensions and Silica Cladding Thickness

Taper geometry and cladding thickness are critical parameters in optimizing mode matching at the coupling interface, as they directly affect mode confinement, field distribution, and the effective refractive index of the taper structure.
By carefully tuning these parameters, it is possible to minimize coupling losses, thereby improving light transfer efficiency between the taper and the fiber. The simulations presented here evaluate the impact of these design factors on coupling performance for both SMFs and lensed fibers. For each fiber type, we analyze the relationship between taper dimensions, cladding thickness, and coupling loss to provide insights into optimal configurations for high-performance photonic interfaces.

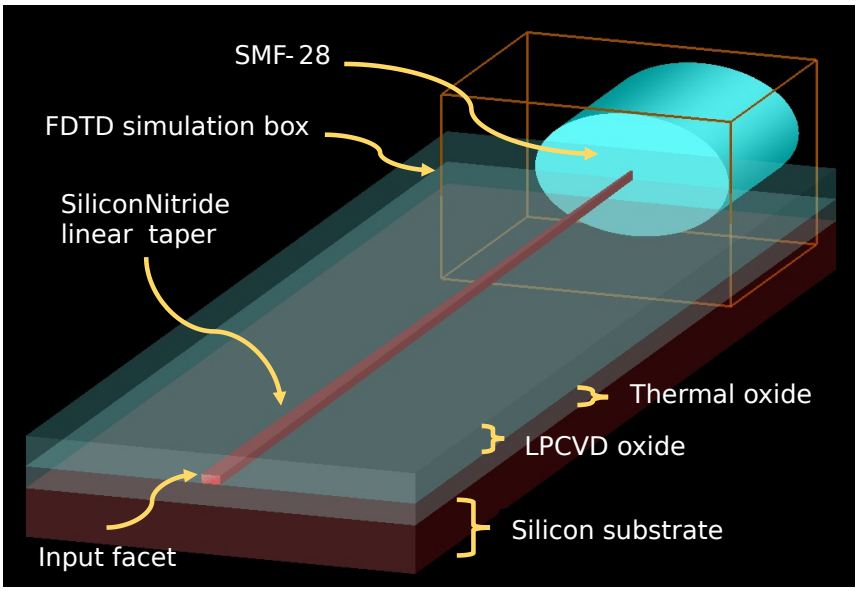

Figure 4.5: Perspective view of the simulation setup for SMF coupling, illustrating the Si3N4 taper configuration. The structure transitions from a wide waveguide to a narrow facet, with a fixed height of 740 nm.

4.3.1 Taper Dimensions and Cladding Thickness Effect on SMF Coupling

To optimize the coupling efficiency between the adiabatic linear Si3N4 taper and a standard single-mode fiber (SMF-28) with a core diameter of 10.4 µm, simulations were conducted to explore the effects of varying taper facet widths and silica (SiO2) cladding thicknesses. The taper height was fixed at 740 nm, a value carefully chosen

to achieve anomalous dispersion for phase matching in nonlinear optics applications. The distance from the edge of the taper to the SMF fiber was also kept at a minimum, representing a 'butt-coupling' condition.

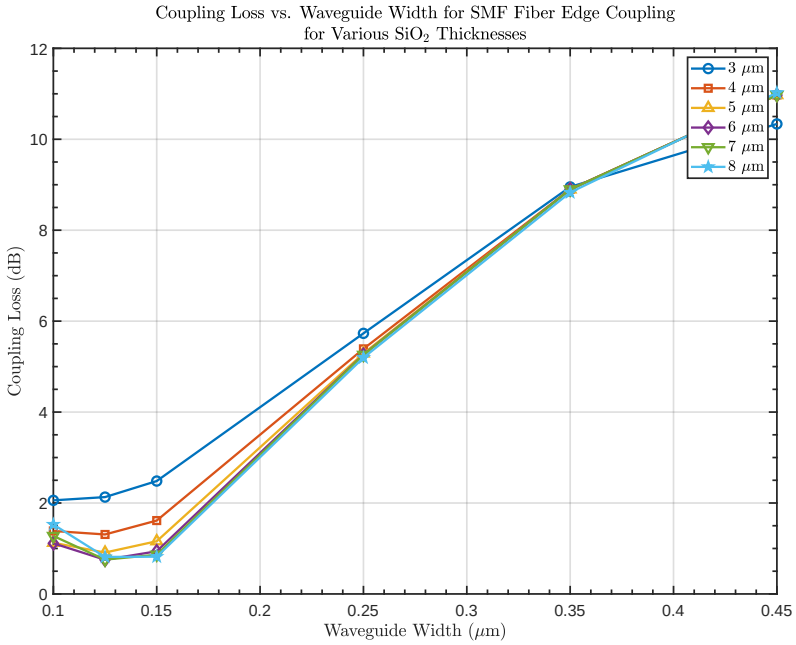

Figure 4.6: FDTD simulation results for SMF coupling, showing coupling loss as a function of taper facet width for varying SiO2 cladding thicknesses. The waveguide height is fixed at 740 nm.

Symmetric SiO2 cladding thicknesses were varied from 3 µm to 8 µm to investigate their influence on coupling efficiency and mode confinement. The cladding consists of a lower thermal oxide layer and an upper LPCVD-deposited oxide layer, both of which are critical for providing vertical optical confinement and reducing substrate leakage. Effective confinement prevents radiation losses and maintains mode symmetry, both of which are crucial for efficient coupling to the SMF.
The simulation results, presented in Figure 4.6, indicate that the optimal coupling loss for SMFs occurs at taper facet widths between 100 nm and 150 nm with 6 µm thick SiO2 cladding layers. Within this range, the coupling loss is minimized to approximately 0.75 dB. Taper widths below 100 nm result in insufficient confinement of the TE mode, as the waveguide dimensions approach the cutoff condition, leading to significant radiation losses. Conversely, widths above 150 nm lead to increased coupling losses due to mode mismatch with the SMF's larger mode field diameter (MFD).
The observed minimal coupling loss in the facet width range of 100 nm to 150 nm is primarily due to the optimal matching of the taper mode's MFD with that of the SMF. At these widths, the effective refractive index (n_{eff}) of the taper mode decreases as the optical field extends more into the cladding. This lateral expansion of the optical mode increases the MFD of the taper mode, enhancing overlap with the SMF's Gaussian mode.

The 6 µm thick SiO2 cladding layers significantly influence mode propagation within the taper. These layers not only provide vertical confinement, preventing leakage into the substrate or air, but also contribute to the effective index contrast that controls lateral mode expansion. This thickness facilitates an ideal MFD for the taper mode, aligning it with that of the SMF for effective coupling. Additionally, the dual-layer configuration, with LPCVD and thermal oxide, minimizes scattering losses, further enhancing mode stability and confinement.

4.3.2 Taper Dimensions and Cladding Thickness Effect on Lensed Fiber Coupling

For coupling with a lensed fiber, the simulations focused on optimizing the coupling efficiency between the adiabatic linear Si3N4 taper and a lensed fiber with a beam waist of 2.5 µm. This beam waist was selected to align with the capabilities of the available experimental setup in the lab environment, ensuring that the simulation results are applicable to real-world conditions.

The taper facet width was varied from 150 nm to 350 nm in steps of 50 nm to assess its influence on coupling efficiency. Initial Finite-Difference Eigenmode (FDE) simulations were conducted to provide an estimate of the ideal coupling conditions by evaluating how well the mode field diameter (MFD) of the taper mode at the edge matches with that of the lensed fiber. The FDE simulations offer an initial approximation, as they do not account for Fresnel reflections but provide insight into the fundamental mode-matching characteristics.

To investigate the influence of cladding thickness, symmetric SiO2 cladding layers were varied between two conditions: a minimum of 3 µm and a maximum of 8 µm. The taper height was fixed at 740 nm, as in the SMF case, to minimize group velocity dispersion and maintain optimal mode confinement.

Following the FDE analysis, a full 3D Finite-Difference Time-Domain (FDTD) simulation was conducted to account for the complete effects of taper dimensions and SiO2 cladding thickness on coupling efficiency. The FDTD results, shown in Figure 4.7, reveal that the minimum optical loss window for the lensed fiber occurs at taper facet widths between 200 nm and 250 nm, with the lowest loss observed at approximately 0.37 dB for a 200 nm facet width with a 3 µm thick symmetric SiO2 cladding layer.

The observed minimal coupling loss within the 200 nm to 250 nm width range can be attributed to optimal mode matching between the taper mode's MFD and the lensed fiber's 2.5 µm beam waist. At these widths, the taper mode's effective index and lateral mode expansion closely align with the beam profile of the lensed fiber, thereby maximizing the mode overlap and minimizing reflection losses. This alignment results in efficient coupling, with the cladding thickness of 3 µm providing sufficient confinement to maintain mode stability and prevent leakage while supporting optimal field overlap.

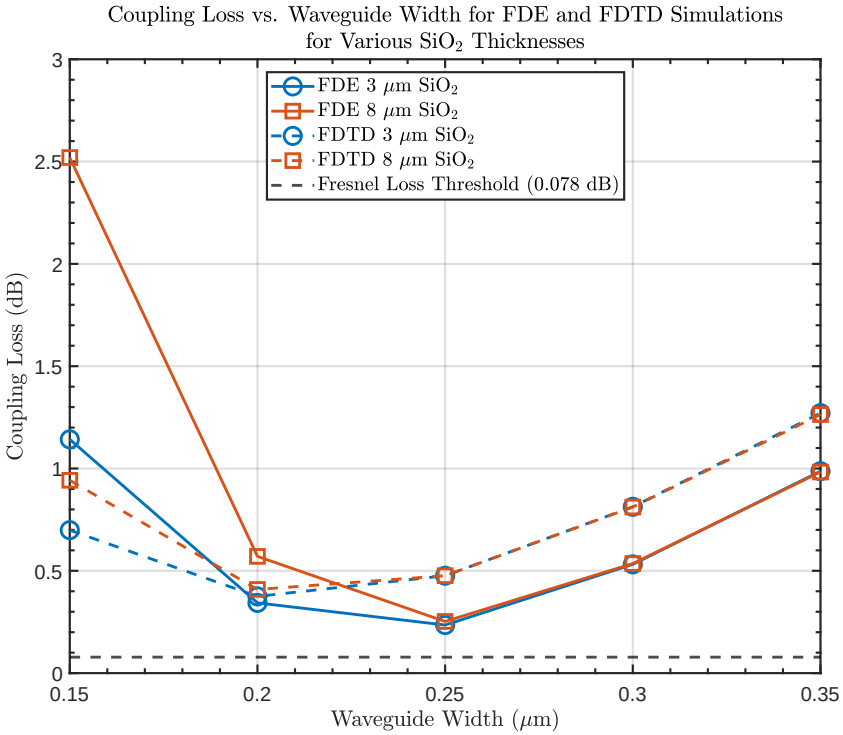

Figure 4.7: FDE and FDTD simulation results for lensed fiber coupling, showing coupling loss as a function of taper facet width for varying SiO2 cladding thicknesses. The waveguide height is fixed at 740 nm.

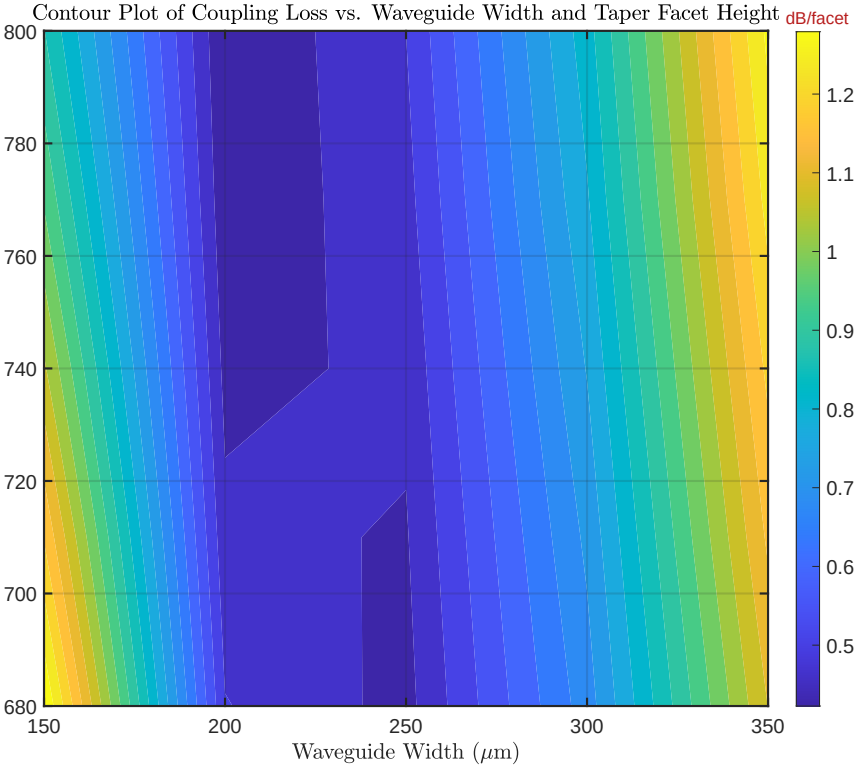

Figure 4.8: Contour plot showing coupling loss as a function of taper facet width and height for lensed fiber coupling. The minimal coupling loss region corresponds to taper widths between 200 nm and 250 nm, with less sensitivity to variations in taper height.

To further understand the impact of the taper height on coupling efficiency, a comprehensive sweep was conducted for both taper height and width to examine their combined effects on coupling loss. The taper height range was chosen based on both manufacturing constraints in the cleanroom environment and the heights that yield minimal dispersion for a confined 1.55 µm wavelength. As shown in Figure 4.8, the coupling loss is more sensitive to changes in taper width than to taper height. This behavior likely arises because the taper width directly influences the lateral mode confinement and MFD matching with the lensed fiber, whereas the height variation within the chosen range has a less significant effect on these critical coupling parameters.
These findings underscore that while height adjustments within the tested range contribute to dispersion minimization, the coupling efficiency is predominantly governed by the taper width, which plays a more critical role in achieving optimal mode field overlap with the lensed fiber.

4.3.3 Experimental Validation of Taper Dimensions for Lensed Fiber Coupling

To complement the simulation results, experimental validation was performed by my supervisor Vijay Shekhawat using a fabricated prototype of the linear taper. The design closely followed the simulation parameters, featuring a silicon nitride (Si3N4) waveguide with symmetric SiO2 cladding layers of 3 µm thickness and a taper height of 740 nm. The experimental setup utilized a lensed fiber with a 2.5 µm beam waist and a laser source operating at 1550 nm with an output power of -1.5 dBm. Both coupling loss per facet and overall insertion loss (fiber-to-chip-to-fiber) were measured for varying taper facet widths.
The results, shown in Figure 4.9, indicate that the lowest coupling loss occurs for facet widths between 230 nm and 290 nm. This experimental observation differs slightly from the FDTD simulation predictions, which identified the lowest coupling loss within the 200 nm to 250 nm range. Despite this slight discrepancy, the coupling loss remains relatively stable, with a variation of no more than 0.5 dB across all tested facet widths. The insertion loss follows a similar trend, further validating the robustness of the taper design.
The slight difference between the experimental and simulated results can be attributed to several factors. Sidewall roughness, introduced during the waveguide fabrication process, likely scattered some light and affected the effective mode field diameter (MFD). Similarly, fabrication imperfections, such as taper width deviations from the design, may have introduced additional variations. Finally, small discrepancies in the refractive index of the Si3N4 and SiO2 layers, due to deposition inaccuracies, may have altered the coupling efficiency.
Overall, the experimental findings corroborate the simulation results, confirming that the taper design is highly tolerant to fabrication imperfections. This tolerance is evidenced by the consistent coupling and insertion losses across a broad range of taper facet widths. The results also suggest that while simulation predicts optimal performance at narrower widths, the experimentally validated range of 230 nm to 290 nm provides a practical, low-loss configuration for real-world implementation.

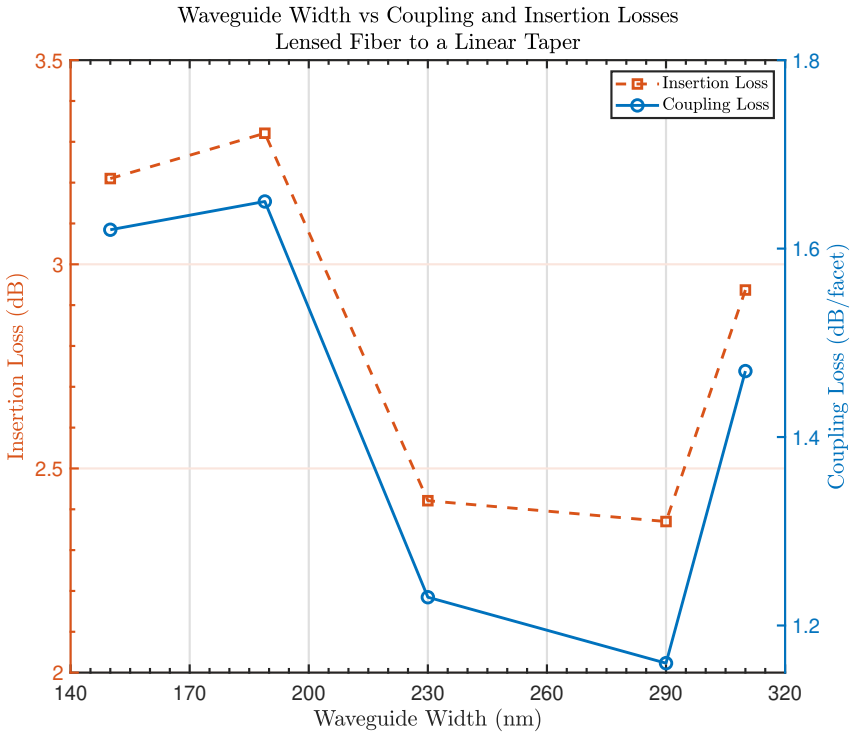

Figure 4.9: Experimental coupling loss and insertion loss vs. taper facet width for lensed fiber coupling. The results indicate that the lowest coupling loss occurs between 230 nm and 290 nm, slightly differing from simulation predictions.

4.3.4 Impact on Design and Fabrication Considerations

The experimental results underscore key insights for future taper design and fabrication. The region between 230 nm and 290 nm constitutes the optimal window for achieving minimal coupling loss while accommodating potential fabrication variances. Furthermore, the narrow range of coupling loss variations highlights the robustness of the design, making it suitable for scalable manufacturing.

4.4 Impact of Taper and Physical Gaps on Coupling Efficiency

In this section, the influence of two distinct gap configurations on the coupling efficiency between the silicon nitride (Si3N4) taper and optical fibers were investigated .The first being the "taper gap," defined as the distance from the end of the taper face to the edge of the chip or substrate on which it is epitaxially grown, and the other being the "physical gap," representing the actual physical separation between the fiber (either SMF or lensed) and the taper structure. The motivation for these simulations stems from the fabrication-induced gap visible in the top-view SEM image of the linear edge taper used in the lab (Figure 1.3), which necessitates accounting

for this feature in FDTD simulations. Additionally, a physical gap is relevant due to potential inaccuracies in fiber alignment during practical implementation.
To illustrate these gap definitions within the simulation environment, Figure 4.10 depicts the taper gap and physical gap as implemented in our models.

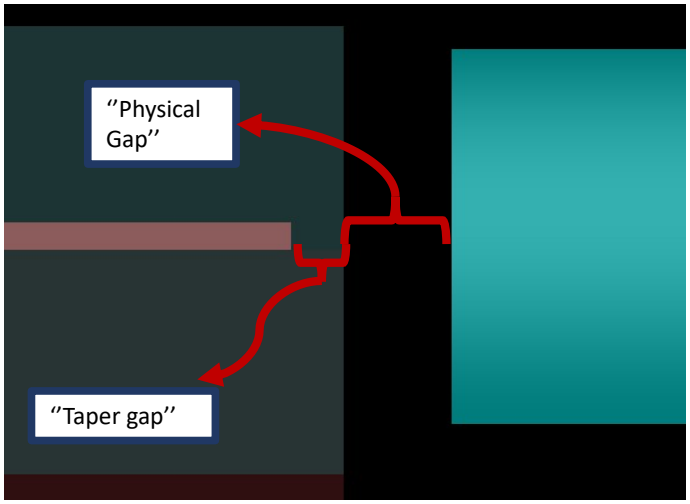

Figure 4.10: Side view illustration of the taper gap and physical gap definitions in the simulation environment

4.4.1 Effect of Gaps on SMF Coupling Efficiency

To evaluate the effect of both taper and physical gaps on SMF coupling efficiency, FDTD simulations were conducted with varying gap distances. The coupling losses were calculated for taper facet widths ranging from 100 nm to 350 nm with a fixed taper height of 740 nm.

4.4.1.1 Taper Gap in SMF Coupling

Figure 4.11 presents the coupling loss as a function of waveguide width for different taper gaps (0 µm, 0.5 µm, 1 µm, and 3 µm). The results indicate that introducing a taper gap of 1 µm slightly reduces the coupling loss for taper widths in the range of 100–150 nm compared to butt coupling (0 µm gap). This improvement is marginal and not significant for wider taper facets. The slight reduction in coupling loss at narrower widths may be attributed to better mode field matching between the SMF and the taper facet when a small gap is introduced.

4.4.1.2 Physical Gap in SMF Coupling

Similarly, the coupling loss for different physical gaps (0 µm, 1 µm, 3 µm, and 5 µm) is shown in Figure 4.12. The results demonstrate that introducing a small physical gap of 1 µm can also lead to a slight reduction in coupling loss within the 100–150 nm taper width range compared to butt coupling. Beyond this width range, the physical gap does not provide any significant benefit and may even increase coupling losses due to reduced mode overlap.

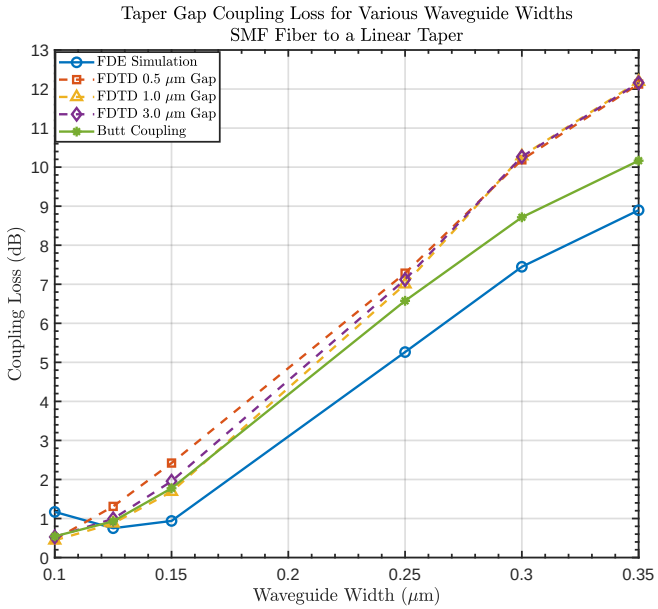

Figure 4.11: Coupling loss (dB) vs. waveguide width for SMF coupling with various taper gaps.

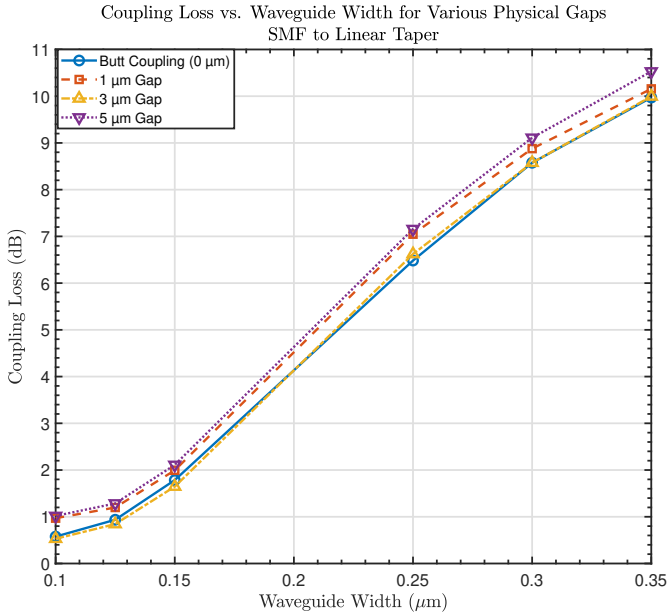

Figure 4.12: Coupling loss (dB) vs. waveguide width for SMF coupling with various physical gaps.

These observations suggest that for narrow taper facets, introducing a small gap may enhance the coupling efficiency by improving mode matching between the taper and the SMF. However, the benefit is minimal and may not outweigh the practical challenges associated with precise gap control during fabrication and alignment.

4.4.2 Taper and Physical Gaps in Lensed Fiber Coupling

Figures 4.13 and 4.14 illustrate the coupling loss as a function of waveguide width for various taper and physical gaps

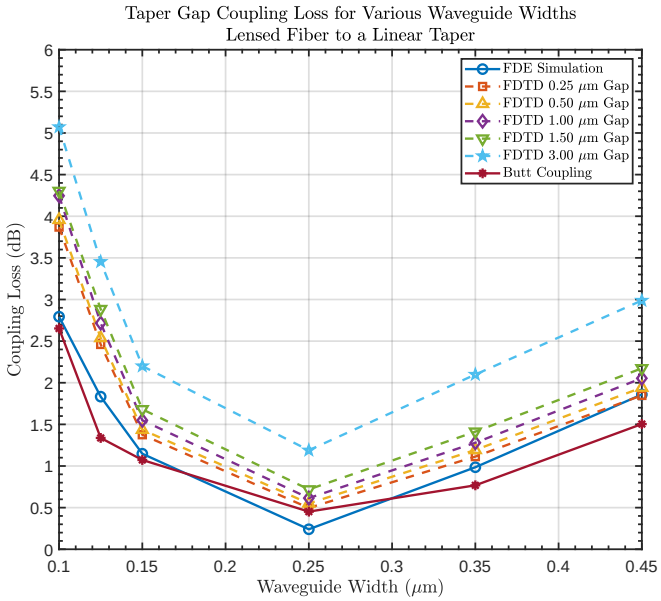

Figure 4.13: Coupling loss (dB) vs. waveguide width for lensed fiber coupling with various taper gaps.

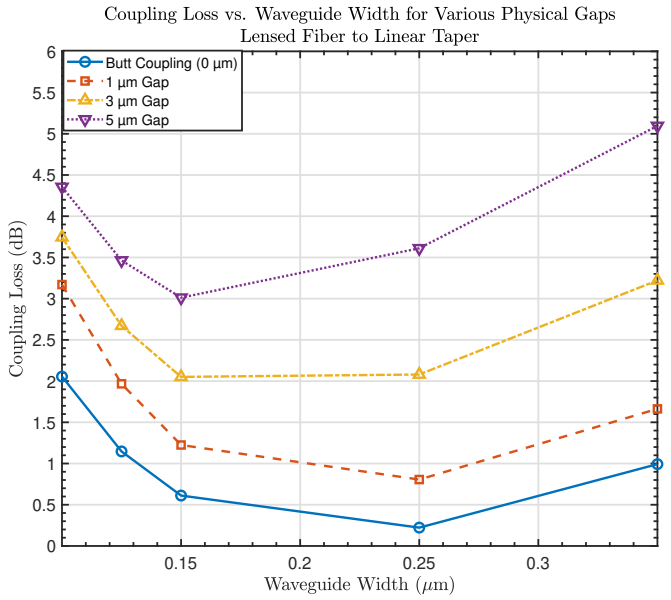

Figure 4.14: Coupling loss (dB) vs. waveguide width for lensed fiber coupling with various physical gaps.

Across all tested waveguide widths, the simulation results consistently show that

butt coupling (0 µm gap) achieves the lowest coupling loss. The simulations were conducted using the Finite-Difference Time-Domain (FDTD) method, with the setup deployed in the simulation environment as illustrated in figure (3.1).The wavelength was set to 1.55µm, and the lensed fiber used in the simulation had a beam waist of 2.5 µm. The taper facet width was fixed at 250 nm, corresponding to the low-loss window for lensed fibers identified in earlier simulations and the height was fixed at 740nm as well.
As the gap increases, the coupling efficiency deteriorates due to reduced mode overlap between the taper facet and the lensed fiber. The larger beam waist of the lensed fiber facilitates optimal mode matching at minimal separation, emphasizing the importance of maintaining small gaps during alignment and fabrication. Introducing either a taper or physical gap generally results in increased losses due to increased divergence and reflection, underscoring the necessity of precise alignment in practical applications.

4.4.3 Experimental Results for Taper Gap in Lensed Fiber Coupling

To complement the simulation findings, the experimental study investigated the effect of the taper gap (facet gap) on coupling loss for lensed fiber coupling. The experimental testing was limited by fabrication constraints, with the smallest taper gap starting at 0.25 µm. A laser source at 1550 nm with an output power of -1.5 dBm and a lensed fiber with a beam waist of 2.5 µm were employed for the measurements.
The experimental results, shown in Figure 4.15, reveal that the coupling loss remains relatively stable across the tested taper gaps, with a difference of approximately **0.1 dB** between the maximum and minimum values. The lowest coupling loss is recorded at a taper gap of **0.5 µm**. Beyond this point, the coupling loss stabilizes, exhibiting an almost constant trend. This behavior suggests that while minimal taper gaps yield the best coupling efficiency, larger gaps beyond **0.5 µm** have a negligible effect on coupling loss.
This indicates a small discrepancy between the simulation and experimental results . In simulations, increasing the taper gap leads to a notable increase in coupling loss due to reduced mode overlap and increased beam divergence between the lensed fiber and the taper facet. However, in the experimental measurements, the coupling loss remains relatively unchanged across different taper gaps.
this discrepancy can be attributed to several factors leading to additional loss mechanisms such as scattering due to sidewall roughness, material absorption, and fabrication-induced defects play a significant role. These losses can overshadow the variations in coupling loss caused by changes in the taper gap. As a result, the overall coupling loss appears relatively insensitive to the taper gap in experiments. Where the simulations assume idealized taper geometries with perfectly smooth surfaces and exact dimensions. In reality, fabrication imperfections lead to deviations in the taper shape and surface quality. These imperfections introduce scattering and absorption losses that are not accounted for in the simulations. Additionally precise alignment between the lensed fiber and the taper facet is challenging to

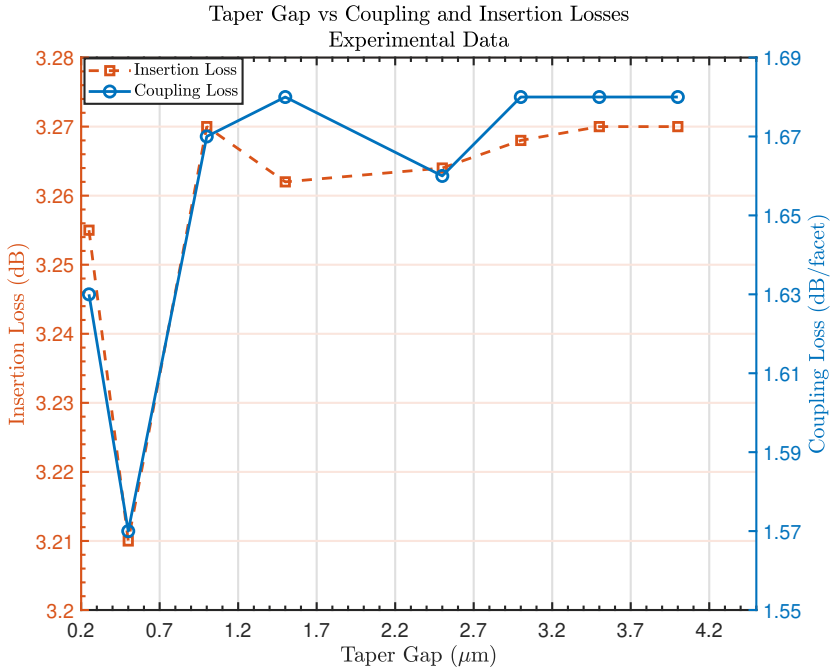

Figure 4.15: Experimental coupling loss (dB) as a function of taper gap for lensed fiber coupling. The minimum coupling loss is observed at a taper gap of 0.5 µm, with negligible variation (∼0.1 dB) for larger gaps.

achieve experimentally. Small misalignments in the lateral or angular positioning can reduce mode overlap and increase coupling losses. These alignment errors can mask the effects of the taper gap on coupling efficiency. On top of that , The experimental apparatus has inherent measurement uncertainties and noise levels that can obscure small variations in coupling loss. The observed difference of approximately **0.1 dB** falls within the typical measurement error margins, making it difficult to conclusively attribute changes in coupling loss to variations in the taper gap.

4.5 Investigation of Beam Divergence on Coupling Efficiency

Another effect investigated in this study was the impact of beam divergence on coupling efficiency, specifically in the context of a lensed fiber configuration. Using a simplified FDTD simulation in Ansys Lumerical, a linear Si3N4 taper (250 nm width by 740 nm height) was coupled to a lensed fiber, and two physical separations—1 µm and 3 µm—were evaluated to observe how beam divergence affects transmission across these gaps.

4.5.0.1 Simulation and Analytical Setup

In the initial setup, termed the "Normal" configuration, direct FDTD simulations were conducted to measure transmission efficiency for each physical gap (1 µm and 3 µm), serving as a baseline without accounting for divergence effects.
To extend this analysis, an analytical approach was applied to simulate the influence of beam divergence over each gap. The divergence angle θ was calculated using Gaussian beam optics principles, as given by:

$$\theta = \frac{\lambda}{\pi w_0} \tag{4.1}$$

where θ is the divergence angle, λ is the wavelength, and w_0 represents the beam waist, or the minimum spot size. These calculated divergence angles were then incorporated into a "Modified" configuration, adjusting the beam profile as it propagated across each physical gap. This setup allowed for a more realistic assessment of transmission by accounting for beam expansion due to divergence.

4.5.0.2 Results and Observations

The transmission results for each physical gap distance, in both Normal and Modified configurations, are presented in Figure 4.16.

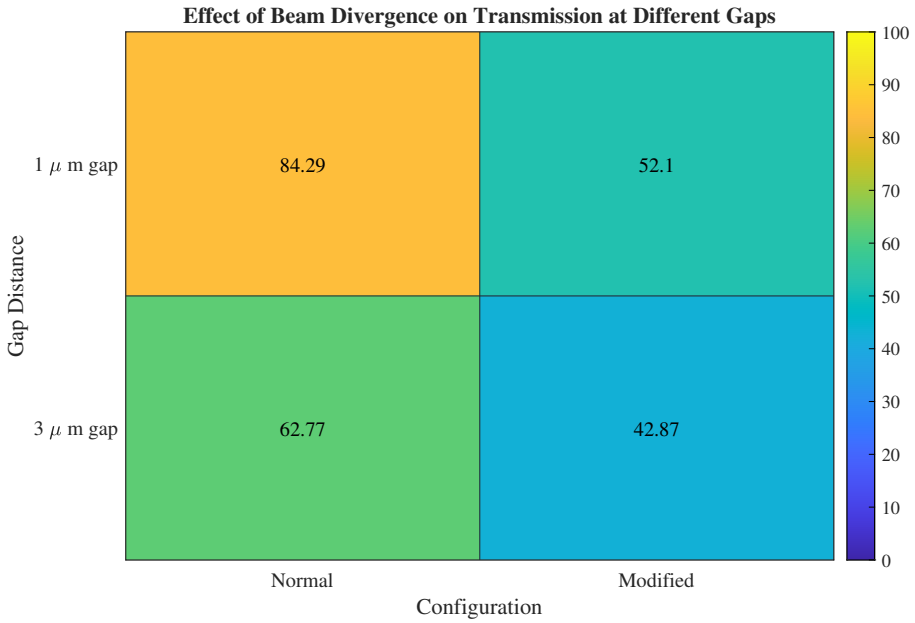

Figure 4.16: Effect of beam divergence on transmission at different physical gaps (1 µm and 3 µm) for both Normal and Modified configurations.

In the Normal configuration, transmission values for the 1 µm and 3 µm gaps were recorded at 84.29% and 62.77%, respectively. However, when beam divergence was taken into account in the Modified configuration, transmission decreased to 52.10% for the 1 µm gap and 42.87% for the 3 µm gap. This reduction highlights the sensitivity of coupling efficiency to beam divergence, particularly as the physical separation increases.

The comparison between the Normal and Modified configurations underscores the significant role of beam divergence in affecting coupling efficiency, especially at larger physical separations. As the gap widens, the Gaussian beam divergence increases, leading to a mismatch between the beam profile and the mode field of the taper facet. This mismatch results in greater scattering and diminished mode overlap, thereby reducing transmission efficiency.
These findings emphasize the importance of minimizing physical gaps in practical implementations to optimize coupling efficiency. Moreover, they highlight the need for precise alignment and control of beam divergence in setups involving lensed fibers coupled to narrow tapers, as divergence-induced losses become increasingly critical with larger separations.

5

Conclusions

5.1 Summary of Key Findings

The integration of photonic components into compact and efficient circuits hinges on effective coupling mechanisms between optical fibers and on-chip waveguides. This thesis has focused on optimizing the coupling efficiency between silicon nitride (Si3N4) waveguides and optical fibers using linear adiabatic edge tapers. Through comprehensive simulations and experimental validation, we have systematically investigated the interplay between taper geometry, cladding thickness, and gap configurations for both standard single-mode fibers (SMFs) and lensed fibers.

One of the primary objectives was to determine the optimal taper length for efficient coupling. Using the Eigenmode Expansion (EME) method, simulations indicated that for SMF coupling, a taper length of approximately **1 mm** is necessary to accommodate the larger mode field diameter (MFD) of the SMF (**10.4 µm**) and ensure adiabatic mode transformation with minimal coupling loss. In contrast, for lensed fiber coupling, both simulations and experimental results confirmed that a taper length of **50 µm** is sufficient to achieve high coupling efficiency. The experimental validation, as presented in Figure 4.3 in Chapter 4, showed minimal variation in coupling and insertion losses across the tested taper lengths, supporting the simulation predictions.

The study revealed the critical role of matching the MFD between the taper facet and the optical fiber to minimize coupling losses. For SMFs, simulations indicated that optimal coupling occurs when the taper facet width is between **100 nm** and **150 nm**, with the lowest coupling loss of approximately **0.75 dB** achieved at **125 nm** (Figure 4.6).

For lensed fibers, simulations predicted an optimal facet width between **200 nm** and **250 nm**, with a minimal coupling loss of **0.37 dB** at **200 nm** (Figure 4.7). However, experimental measurements indicated a slightly wider optimal range between **230 nm** and **290 nm**, with the lowest coupling loss of **1.1 dB per facet** observed at **290 nm** (Figure 4.9) which can be reduced even further potentially. The slight discrepancy between simulations and experiments may be due to fabrication imperfections, such as sidewall roughness and taper dimension deviations, which may have affected the effective MFD and coupling efficiency.

The importance of cladding thickness was also confirmed. For SMF coupling, a symmetric SiO2 cladding thickness of **6 µm** provided robust vertical confinement, reducing substrate leakage and facilitating optimal mode expansion. For lensed fiber coupling, a thinner cladding of **3 µm** was sufficient to support effective mode

overlap with the fiber's beam waist.
The effects of taper gap (the distance from the taper facet to the edge of the substrate) and physical gap (the separation between the fiber and the taper facet) on coupling efficiency were thoroughly investigated. For SMF coupling, simulations showed that introducing a taper gap of **1 µm** slightly reduced coupling loss for taper widths between **100 nm** and **150 nm**, compared to butt coupling with no gap (Figure 4.11). Similarly, small physical gaps up to **1 µm** led to marginal improvements in coupling efficiency due to enhanced mode matching.
In contrast, for lensed fiber coupling, both simulations and experimental results emphasized the necessity of maintaining minimal gaps. Simulations demonstrated that any increase in taper or physical gap resulted in higher coupling losses due to reduced mode overlap and increased beam divergence (Figures 4.13 and 4.14). Experimental testing corroborated these findings, showing that the coupling loss remained relatively stable, with the lowest loss observed at a taper gap of **0.5 µm**, and negligible variations for larger gaps (Figure 4.15). This stability suggests that while minimal gaps are ideal, the design is tolerant to small fabrication-induced gaps.
Beam divergence was identified as a significant factor affecting coupling efficiency, particularly for lensed fiber configurations with physical gaps. Simulations incorporating beam divergence effects showed a substantial decrease in transmission efficiency with increasing gap size. For instance, at a physical gap of **1 µm**, transmission efficiency decreased from **84.29%** to **52.10%** when beam divergence was considered (Figure 4.16). These results highlight the importance of precise alignment and minimizing physical gaps to mitigate divergence-induced losses.
The findings of this research have significant implications for the design and fabrication of photonic integrated circuits (PICs) utilizing silicon nitride waveguides. The identification of optimal taper geometries and dimensions enables the development of efficient fiber-to-chip coupling interfaces, which are crucial for high-performance optical communication systems. The demonstrated robustness of the taper design to fabrication imperfections and its tolerance to small gaps facilitate scalable manufacturing processes, enhancing the practicality of integrating PICs into commercial applications.
Furthermore, the integration of simulation and experimental validation provides a comprehensive understanding of the coupling mechanisms, allowing for more accurate predictions and optimizations in future designs. The insights into the effects of cladding thickness, taper gap, and beam divergence contribute to the broader knowledge base in the field, informing best practices for PIC development.

5.2 Limitations of the Study

While the study yielded valuable results, certain limitations must be acknowledged. The simulations did not fully account for all real-world fabrication imperfections. Factors such as sidewall roughness, observed to be around **50 nm** in SEM images, and variations in material refractive indices due to deposition inconsistencies were not explicitly modeled. These imperfections likely contributed to the discrepancies between simulated and experimental results, particularly in the observed coupling

losses for lensed fiber coupling.
The study focused on a single wavelength of **1550 nm**, corresponding to the telecom C-band where silicon nitride exhibits low optical loss. Consequently, the performance of the taper design over a broader wavelength range was not evaluated. Applications requiring broadband operation may necessitate additional analysis to ensure consistent coupling efficiency across multiple wavelengths.
Additionally, the lensed fiber was modeled as an ideal Gaussian beam source in simulations. Real-world lensed fibers may exhibit aberrations or deviations from the ideal profile, potentially affecting coupling efficiency. Experimental limitations, such as the minimum achievable taper gap of **0.25 µm** due to fabrication constraints, restricted the validation of simulated performance at smaller gap sizes.

6
Future Work

6.1 Suggestions for Further Research

Building upon the findings of this study, several avenues for further research can enhance the understanding and application of optimized coupling structures in photonic integrated circuits. One significant direction is the exploration of the coupling efficiency over a broader wavelength range. While this study focused on the telecommunications wavelength of 1550, extending the analysis to cover other wavelengths, such as the 1310 window or even into the visible spectrum, could expand the applicability of the taper designs to a wider range of optical systems, including biomedical imaging and sensing applications.

Investigating the polarization dependence of the coupling efficiency is another critical area. The simulations in this study primarily considered the fundamental TE mode, but in practical applications, polarization diversity and polarization-dependent losses can significantly impact system performance.

The simulation methods employed in this study, while robust, relied on certain assumptions and simplifications. Future studies could refine these methods by incorporating more advanced modelling techniques that account for fabrication-induced imperfections such as sidewall roughness, and material inhomogeneities. Utilizing stochastic modelling or Monte Carlo simulations can provide a statistical understanding of how these imperfections affect coupling efficiency, leading to designs that are more tolerant to fabrication variances.

Lastly, Integrating thermal and mechanical effects into the simulations is another area for enhancement. Since photonic devices can be sensitive to temperature changes and mechanical stresses, which can alter refractive indices and physical dimensions, impacting performance. By including thermo-optic and stress-optic effects in the simulations, it is possible to predict the behavior of the taper under varying environmental conditions, leading to more robust designs suitable for real-world applications.

Bibliography

[1] M. K. Smit, J. J. G. M. van der Tol, and M. T. Hill, "Moore's Law in Photonics," *Laser & Photonics Reviews*, vol. 13, no. 1, p. 1800225, 2019.

[2] B. E. A. Saleh and M. C. Teich, *Fundamentals of Photonics*, 2nd ed. Hoboken, NJ, USA: Wiley, 2007.

[3] D. A. B. Miller, "Attojoule optoelectronics for low-energy information processing and communications," *Journal of Lightwave Technology*, vol. 35, no. 3, pp. 346–396, Feb. 2017.

[4] J. Sun *et al.*, "Single-chip microprocessor that communicates directly using light," *Nature*, vol. 528, no. 7583, pp. 534–538, Dec. 2015.

[5] L. Vivien and L. Pavesi, Eds., *Handbook of Silicon Photonics*. Boca Raton, FL, USA: CRC Press, 2016.

[6] Cisco Visual Networking Index: Forecast and Trends, 2017–2022, White Paper, Cisco Systems, Nov. 2018. [Online]. Available: `https://www.cisco.com/c/en/us/solutions/collateral/service-provider/visual-networking-index-vni/white-paper-c11-741490.html`

[7] L. Chrostowski and M. Hochberg, *Silicon Photonics Design: From Devices to Systems*. Cambridge, U.K.: Cambridge University Press, 2015.

[8] J. E. Bowers, "Integration of photonics and electronics," *Proceedings of the IEEE*, vol. 107, no. 7, pp. 1431–1437, Jul. 2019.

[9] J. G. Fujimoto and E. A. Swanson, "The development, commercialization, and impact of optical coherence tomography," *Investigative Ophthalmology & Visual Science*, vol. 57, no. 9, pp. OCT1–OCT13, Jul. 2016.

[10] R. Hui and M. O'Sullivan, *Fiber Optic Measurement Techniques*. Waltham, MA, USA: Academic Press, 2009.

[11] X. Guo, "Surface plasmon resonance based biosensor technique: A review," *Journal of Biophotonics*, vol. 5, no. 7, pp. 483–501, Jul. 2012.

[12] W. Bogaerts *et al.*, "Silicon microring resonators," *Laser & Photonics Reviews*, vol. 6, no. 1, pp. 47–73, Jan. 2012.

[13] J. W. Silverstone *et al.*, "Silicon quantum photonics," *IEEE Journal of Selected Topics in Quantum Electronics*, vol. 22, no. 6, pp. 390–402, Nov. 2016.

[14] M. J. R. Heck, "Highly integrated optical phased arrays: Photonic integrated circuits for next-generation LiDAR systems," *Proceedings of SPIE*, vol. 10923, p. 1092306, Feb. 2019.

[15] J. Wang, F. Sciarrino, A. Laing, and M. G. Thompson, "Integrated photonic quantum technologies," *Nature Photonics*, vol. 14, no. 5, pp. 273–284, May 2020.

[16] M.-C. Amann and T. Bosch, "Lidar: Survey of technologies and applications," in *Proceedings of SPIE*, vol. 10026, p. 1002602, Jan. 2017.

[17] W. S. Zaoui *et al.*, "Bridging the gap between optical fibers and silicon photonic integrated circuits," *Optics Express*, vol. 22, no. 2, pp. 1277–1286, Jan. 2014.

[18] H. Bao *et al.*, "Review of optical waveguide taper technology," *Nanophotonics*, vol. 7, no. 9, pp. 1391–1416, Sep. 2018.

[19] R. Bozovich and M. Aziz, "Reliability and lifetime of photonic devices for harsh environments," *NEPP Electronic Technology Workshop*, 2022. [Online]. Available: `https://nepp.nasa.gov/docs/etw/2022/14-JUN-TUE/1515-Bozovich-Aziz-CL-22-2822.pdf`

[20] L. Cheng *et al.*, "Grating couplers on silicon photonics: Design principles, emerging trends and practical issues," *Micromachines*, vol. 11, no. 7, p. 666, Jul. 2020.

[21] L. Chen, K. Preston, S. Manipatruni, and M. Lipson, "Integrated inverse-tapered coupling for low-loss silicon-on-insulator waveguides," *IEEE Photonics Technology Letters*, vol. 22, no. 15, pp. 1156–1158, Aug. 2010.

[22] G. Roelkens, D. Van Thourhout, and R. Baets, "Silicon-on-insulator photonic integrated circuits for the near-infrared and mid-infrared wavelength range," *Journal of the Electrochemical Society*, vol. 157, no. 6, pp. B743–B749, 2010.

[23] V. R. Almeida, R. R. Panepucci, and M. Lipson, "Nanotaper for compact mode conversion," *Optics Letters*, vol. 28, no. 15, pp. 1302–1304, Aug. 2003.

[24] P. Bienstman and R. Baets, "Optical modelling of photonic crystals and VCSELs using eigenmode expansion and perfectly matched layers," *Optical and Quantum Electronics*, vol. 33, no. 4–5, pp. 327–341, Apr. 2001.

[25] A. W. Snyder and J. D. Love, *Optical Waveguide Theory*. London, U.K.: Chapman and Hall, 1983.

[26] Y. Ding, C. Peucheret, H. Ou, and K. Yvind, "Efficient all-silicon polarization splitting and rotating device for silicon-on-insulator platform," *Optics Letters*, vol. 39, no. 18, pp. 5348–5350, Sep. 2014.

[27] A. F. Oskooi *et al.*, "MEEP: A flexible free-software package for electromagnetic simulations by the FDTD method," *Computer Physics Communications*, vol. 181, no. 3, pp. 687–702, Mar. 2010.

[28] A. Taflove and S. C. Hagness, *Computational Electrodynamics: The Finite-Difference Time-Domain Method*, 3rd ed. Norwood, MA, USA: Artech House, 2005.

[29] S. Park, S. Rim, J. W. Kim, J. Park, I.-B. Sohn, and B. H. Lee, "Analysis of design and fabrication parameters for lensed optical fibers as pertinent probes for sensing and imaging," *Sensors*, vol. 18, no. 12, p. 4150, Dec. 2018.

DEPARTMENT OF MICROTECHNOLOGY AND NANOSCIENCE
CHALMERS UNIVERSITY OF TECHNOLOGY
Gothenburg, Sweden
www.chalmers.se

CHALMERS
UNIVERSITY OF TECHNOLOGY